İZMİR
KÂTİP ÇELEBİ
ÜNİVERSİTESİ
2010
GRADUATE SCHOOL OF NATURAL
AND APPLIED SCIENCES

Printed Circuit Board Coil Based Electromagnetic Actuator Design For Micro/Milliscale Manipulation

Submitted to the Graduate School of Natural and Applied Sciences
in partial fulfillment of the requirements for the degree of

Master of Science

in Robotics Engineering

by
Erdem Doguş AKKUŞ

July, 2023

This is to certify that we have read the thesis **Printed Circuit Board Coil Based Electromagnetic Actuator Design for Micro/Miliscale Manipulation** submitted by **Erdem Doguş Akkuş**, and it has been judged to be successful, in scope and quality, at the defense exam and accepted by our jury as a MASTER'S THESIS.

APPROVED BY:

Advisor: **Prof. Dr. Levent Çetin**
İzmir Kâtip Çelebi University

Committee Members:

          Prof. Dr. Levent Çetin
İzmir Kâtip Çelebi University

          Assist. Prof. Dr. Özgür Tamer
Dokuz Eylül University

          Assist. Prof. Dr. Nail Akçura
İzmir Kâtip Çelebi University

Date of Defense: July 12, 2023

Declaration of Authorship

I, **Erdem Doguş Akkuş**, declare that this thesis titled **Printed Circuit Board Coil Based Electromagnetic Actuator Design for Micro/Miliscale Manipulation** and the work presented in it are my own. I confirm that:

- This work was done wholly or mainly while in candidature for the Master's degree at this university.
- Where any part of this thesis has previously been submitted for a degree or any other qualification at this university or any other institution, this has been clearly stated.
- Where I have consulted the published work of others, this is always clearly attributed.
- Where I have quoted from the work of others, the source is always given. This thesis is entirely my own work, with the exception of such quotations.
- I have acknowledged all major sources of assistance.
- Where the thesis is based on work done by myself jointly with others, I have made clear exactly what was done by others and what I have contributed myself.

Date: 12.07.2023

_____

Printed Circuit Board Coil Based Electromagnetic
Actuator Design for Micro/Milliscale Manipulation

Abstract

Trends in nano and micro technologies have directed researchers' concern towards designing small-scale functional systems, i.e., MEMS, NEMS, etc. This study represents a design and implementation scheme for a class of small-scale actuators. Electromagnetic actuators currently used have disadvantages in small-scale applications since they cannot be produced in the desired sizes and compactness due to complex components. Using printed circuit board (PCB) based design strategies, scalable actuators can be produced in a smaller form factor and at a lower cost. The study aims to produce planar PCB actuators that are relatively simple, consisting of fewer discrete parts, producible in a single plant, and are in reduced-size dimension. Another advantage of the PCB-based design is that the control and power electronics can be embedded in the actuator. With these goals, the design steps in the project can be listed as follows: First, designing a coil that consists of copper paths on the PCB that can meet the expectations (homogeneous magnetic field, high magnetic force/current ratio), then building a planar actuator using these coil structures. As the final step, designing the control structure and circuitry suitable for the actuator and its integration into the system. The proposed systesm test results shows that, the PCB coil actuator could apply a force of up to 10 mN to the 1.55 mm microrobot and position it with an uncertainty of 120 μm.

Keywords: PCB Based Coils, Electromagnetic Actuators, Micro/Macro Manipulation.

Mikro/Mili Ölçekli Manipülasyon için Baskı Devre Tabanlı Elektromanyetik Aktüatör Tasarımı

Öz

Nano ve mikro teknolojilerdeki eğilimler, araştırmacıların ilgisini küçük ölçekli (MEMS, NEMS, vb.) işlevsel sistemler tasarlamaya yöneltmiştir. Bu çalışma, küçük ölçekli eyleyiciler sınıfı için bir tasarım ve uygulama şemasını temsil etmektedir. Halihazırda kullanılan elektromanyetik eyleyiciler, karmaşık yapı parçaları nedeniyle istenilen boyut ve kompaktlıkta üretilemedikleri için küçük ölçekli uygulamalarda dezavantajlara sahiptir. PCB tabanlı tasarım stratejileri kullanılarak, ölçeklenebilir aktüatörler daha küçük form faktöründe ve daha düşük maliyetle üretilebilir. Çalışmanın amacı nispeten basit, daha az ayrık parçadan oluşan, tek bir tesiste üretilebilen ve küçük boyutlu düzlemsel PCB eyleyicileri üretmektir. PCB tabanlı tasarımın bir diğer avantajı da kontrol ve güç elektroniğinin aktüatör üzerine gömülebilmesidir. Bu hedefle projede tasarım adımları şu şekilde sıralanabilir; Öncelikle PCB üzerinde bakır yollardan oluşan ve beklentileri karşılayabilecek (homojen manyetik alan, yüksek manyetik kuvvet/akım oranı) bir bobin tasarlayabilmek, Sonrasında bu bobin yapılarını kullanarak düzlemsel bir eyleyici oluşturmak. Son olarak eyleyiciye uygun konrol devresinin tasarlanıp sisteme entegre edilmesidir. Gerçekleştirilen testlerde, PCB bobin eyleyicin 1.55 mm boyutundaki mikrorobota 10 mN kadar kuvvet uygulayabildiğini ve 120 μm bir belirsizlik ile konumlandırabildiği ortaya koymuştur.

Anahtar Kelimeler: PCB Tabanlı Bobinler, Manyetik Eyleyiciler, Mikro/Makro Manipülasyon

v

Acknowledgement

Table of Contents

List of Figures

List of Tables

List of Abbreviations

PCB	Printed Circuit Board
MEMS	Micro electro-mechanical systems
NEMS	Nano electro-mechanical systems
RFID	Radio-frequency identification
DC	Direct current
IPC	Institute for Printed Circuits
PCBA	Printed Circuit Board Assembly
FR4	Fire Resistant Four
LCR	Inductance (L), capacitance (C), and resistance (R)
FEM	Finite Element Method
SMD	Surface Mount Design
IC	Integrated Circuit
MOSFET	Metal Oxide Semiconductor Field Effect Transistor
PWM	Pulse Width Modulation
LED	Light Emitting Diode
USB	Universal Serial Bus
CAD	Computer-Aided Design

List of Symbols

R	Resistance (Ω)
C	Capacitance (F)
L	Inductance (H)
i	Current (A)
Q	Quality Factor
P_{loss}	Power Loss (W)
a	Temperature Coefficient (K^{-1})
ρ	Specific Resistivity ($\Omega \cdot m$)
μ_0	Vacuum Permability ($N. A^{-2}$)
σ	Conductivity ($\Omega.m$)
H	Magnetic Field Strength (A/m)
B	Magnetic Flux Density (T)
F	Force (N)
V	Volume (m^3)
M	Magnetization Vector (A/m)
χ_p	Magnetic Susceptibility ($m^3. kg^{-1}$)
C_d	Drag Coefficient
Vel	Velocity (m/s)

Chapter 1

1. Introduction

1.1 Relevance of Research

Today, the demand for small and more specialised electronic devices leads the electronics industry to manufacture compact appliances. The related developments bring new challenges, requiring the small components to be grasped without damage and then transported to the desired assembly area [1,2,3]. Such problems are also valid for systems operating in the laboratory environment because working with micro-nano-sized particles in the laboratory environment renders conventional processes ineffective. Such requirements have increased the trends in nano and micro technologies and directed the attention of researchers to design functional assembly systems on a small scale, i.e., MEMS, NEMS and so on.[4,5,6].

Along with the decreasing production dimensions and the shrinkage of the manufactured components or the nature of the particle created in the laboratory environment, new handling devices that can carry these components also require smaller and more sensitive actuators. However, the conventional actuators used today have disadvantages in small-scale applications as they cannot be produced in the desired scale due to complex structural parts. As the actuator components get smaller, the strength of the material becomes a limiting factor, and the production and material costs increase as more authentic materials are tried to be produced. Therefore, non-contact actuators[7] attract the attention of users.

Untethered actuator types can be classified as: magnetic, electrostatic, optics, Bernoulli, air cushing, standing wave, and near field. They are designed to serve a very similar purpose. In this context, a magnetic contactless actuator is studied for

the project. The push-pull forces are generated using the magnetic field[8,9,10] by the magnet. The magnetic field can be generated using three different sources: permanent magnets, electromagnets and superconducting magnets. Electromagnet-permanent magnet configurations are the most widely used actuators.

1.2 Motivation and Scope of the Study

The motivation of this study is to create a new, more efficient, and cost-efficient alternative to planar solenoid-based actuators using PCB-based coil design methods for contactless handling or assembly. Since conventional wire wound-based coil is rather bulky and very hard to produce in small sizes (10mm and lower sizes and with 0.1 mm wire diameter), wires need to be very thin at that dimension and can brake easily. PCB production methods tend to give better yields at lower sizes with thinner copper and thanks to photolithography PCB manufacturing, various coil shapes can be made.

In traditional systems, electromagnets are formed by wrapping enamel-coated coil wires around the silica sheet. The components are manufactured in different production facilities and finally assembled with the desired properties. Each step-in production increases the production time and cost. Considering that an electromagnet is obtained when current is passed over a coiled conductive object to form a coil, the coil design to be made with copper paths on the PCB and then its use as an electromagnet makes it possible. Refenrencing to the recent developments in the PCB production market, paths of 75 µm width and 35 µm height can be produced, and with the increase in the number of manufacturers (resulting a contest in global market for the customers.), the production costs and steps are reduced. Thus, using PCB-based design strategies, actuators can be manufactured in a smaller form factor and cost less. Another advantage of PCB-based design is that control and power electronics can be embedded in the actuator, bringing the discrete components in the system into a single whole, further reducing costs and production times.

The considered coils in the project consist of copper paths on the PCB and they form an electromagnet which will be the main actuation units of the actuator. By changing the current on the conductors of electromagnets, the magnetic field produced by the magnet can be controlled so that magnetic or ferromagnetic particles[11,12,13] can be moved.

1.3 Literature Survey

PCBs are generally used to provide the electrical connection between the passive or active electronic components they are on and provide a mechanical body due to their solid structure. It takes the form of a laminate sandwich structure of conductive(copper) and insulating layers. Each of the conductive layers is designed with a pattern of traces, planes, and other features etched from one or more layers of sheet metal. Copper laminated over and/or between layers of non-conductive base material foils. Electrical components may be installed on conductive pads at external junctions designed to accept component terminals, often by soldering, for both electrical connections and mechanical attachment.

Since PCB manufacturing is a combination of mechanical and chemical PCB production is a multistage process that includes many steps. But if we consider the technological and physical development of the PCB production sector in recent years, it has been much easier and more accessible to design and produce a PCB than a solenoid or a motor.Common PCB manufacturing technology has risen to a point that PCBs can come out of a single factory or even a single line.

However designers and researchers have discovered that PCBs can be used for other purposes as well. Radial and linear actuators, voice coils, valves and pumps comprise some of the applications. Producing actuators on PCB is not a very new concept. Studies on PCB-based actuators emerged in the late 1990s and early 2000s. A miniature pump example can be seen in Figure 1.1.
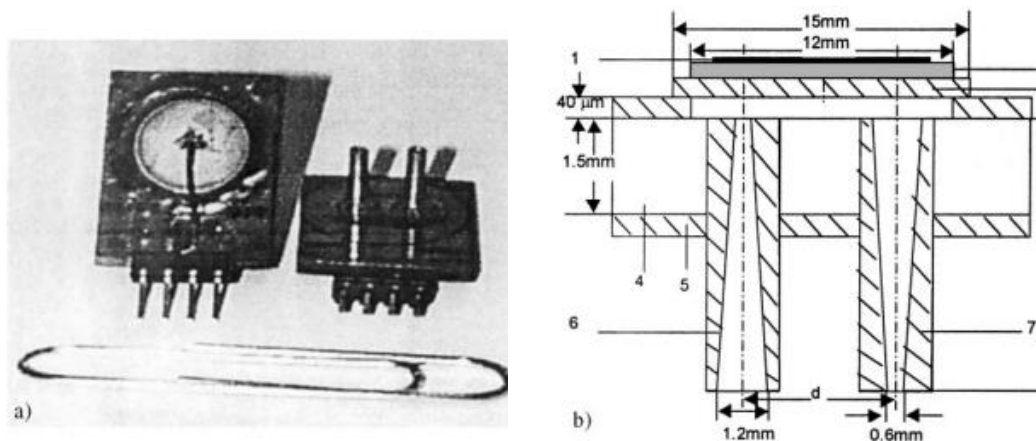
Figure 1.1: Miniature valveless pumps based on printed circuit board [14]

The first studies in this field focused on micro/miliscale actuators that were hard to produce with conventional methods of the era. Even if there is still no commercial products available in that area, researchers, and designers study PCB-based actuators for various purposes. Today, it is very common to prefer between 2 and 10 layers of PCBs in commercial products, however they can have up to 32 layers of copper. However, the first PCBs generally consisted of one or two layers. Thus, when designers wanted to add a coil or similar embedded component on the PCB, they were uable to have more layers. Due to these design constraints, designers had to use so-called planar type coils (spiral inductors).
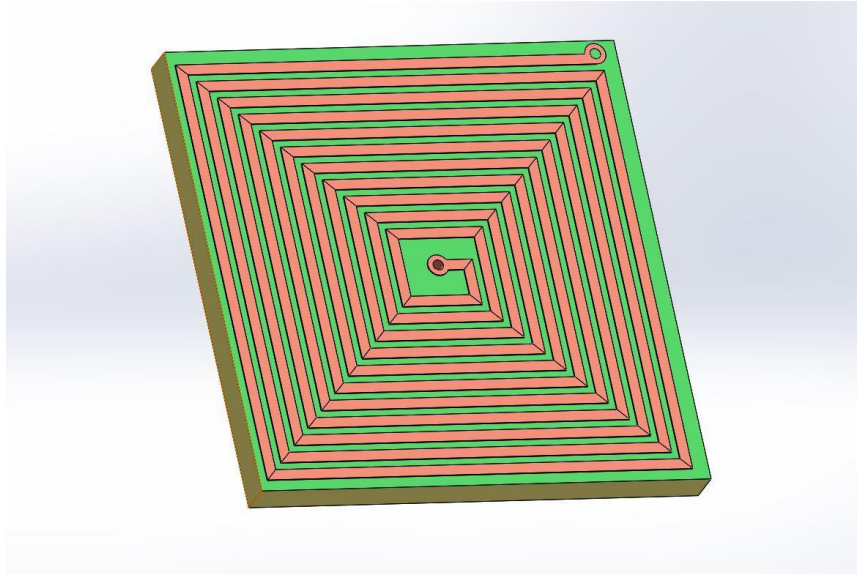
Figure 1.2: PCB square planar coil

Planar coils shown in Figure 1.2, also known as planar spiral coils or flat spiral coils, are a type of electromagnetic coil used in various applications such as wireless power transfer, RFID, biomedical devices, and planar actuators given Figure 1.3. One of the key advantages of planar coils[15,16] is their flat geometry, which makes them suitable for applications where a low profile is desired. This shape also enables them to be easily fabricated using PCB technology.
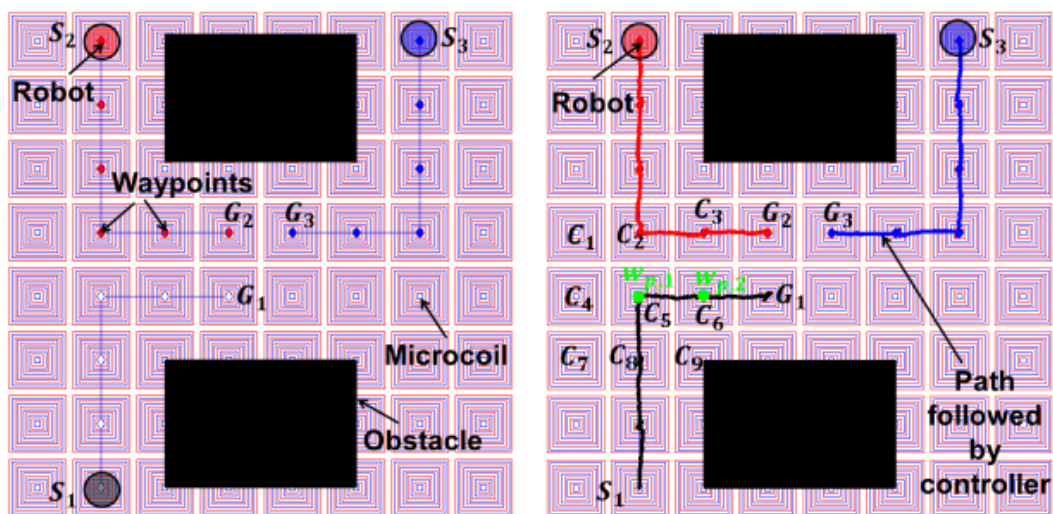
Figure 1.3: PCB planar actuator[17]

Though, planar coils typically have lower inductance compared to other types of coils, such as solenoidal coils. The reason is that the turns of the coil are distributed over a larger area, which reduces the magnetic field strength. Despite this drawback, planar coils have a higher coupling coefficient between coils compared to other types of coils. The flat spiral shape allows for more efficient coupling of the magnetic fields, resulting in better transfer of power or information between coils.

Another characteristic of planar coils is their directional radiation pattern. The magnetic field is strongest in the plane of the coil and weakest perpendicular to it. This directional radiation pattern makes planar coils particularly suitable for applications where focused energy transfer is desired.
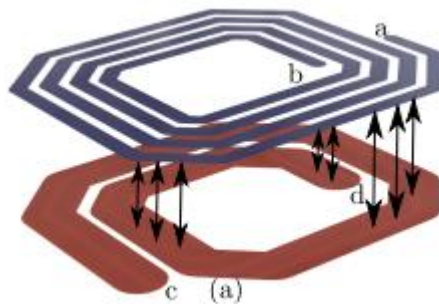
Figure 1.4: Planar coils for wireless power transfer[18]

However, planar coils shown in Figure 1.4 also have a limited range for wireless power transfer[18] and communication applications. This is due to the low inductance and directional radiation pattern, which can result in a weaker magnetic field and lower efficiency at longer distances. Nonetheless, planar coils can be easily customized to meet specific application requirements. The number of turns, the shape and size of the coil, and the spacing between turns can all be adjusted to optimize performance for a given application.

In summary, planar coils have a unique combination of advantages and disadvantages that make them suitable for specific applications. Their flat geometry

and efficient coupling of magnetic fields make them ideal for low-profile applications, while their directional radiation pattern enables focused energy transfer. However, their limited range and lower inductance must be considered when designing a system that utilizes planar coils.

In this study it the aim is develop a PCB-based contactless electromagnetic actuation drive for milli/micro scale movements. According to this goal, the following design objectives were taken in to consideration:

- To design a PCB-based flat coil for repulsion of millimetre-scale permanent magnet or magnetic particle (with dimensions of 1-10 mm diameter)
- To compare the theoretical model and physical prototype of the designed planar coil.
- To design a proof-of-concept PCB coil-based electromagnetic actuator.
- To produce the designed drive and experimentally derive its characteristics (maximum speed, positioning repeatability and accuracy).

Chapter 2

2. Design of PCB Coils

The systematic design process of PCB coils designed for usage in the thesis is provided in this chapter. Structural, thermal, and magnetic properties of PCB coils were examined, and analytical calculations and simulations were used to check for appropriateness for use in electromagnetic actuator design.

2.1 PCB Coils Design Principles

The design of PCB coils revolves around achieving the desired inductance value while minimizing losses and maximizing performance. Key considerations in PCB coil design include selecting the appropriate core material, determining the number of turns, and optimizing shape and size of the coil. The choice of core material, such as ferrite or powdered iron, influences the inductance, saturation, and frequency response of the coil. The number of turns affects the inductance value and its ability to handle high currents of the coil. By carefully designing the shape and size of the coil, designers can control its magnetic field distribution and minimize parasitic capacitance and resistance. Overall, understanding these design principles enables engineers to create PCB coils that satisfy specific requirements and deliver efficient and reliable performance in electronic circuits.

2.1.1 Mathematical Model of a PCB Coil

A real coil model can be represented as a combination of ideal components hence its effect on the circuit is not a single inductive reactance but an impedance. The electrical model and the related coil shapes are given in Figure 2.1.

| (a) | (b) |
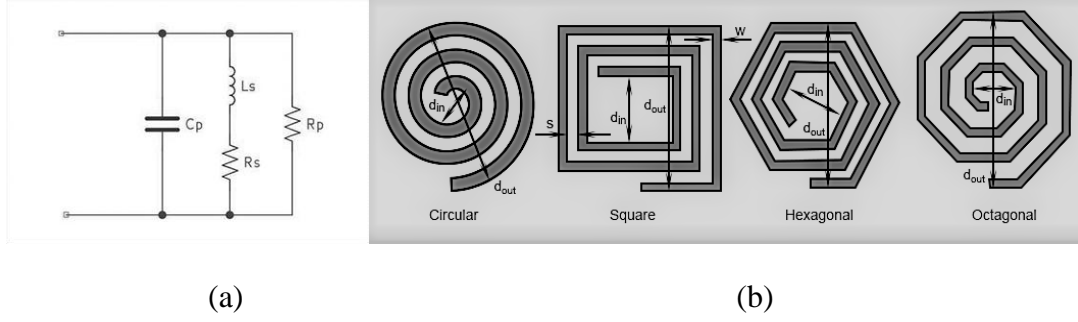
Figure 2.1: Model of PCB Coil (a), Planar Coil Types (b)

The mathematical model of the system can be obtained using Kirchhoff's Current Law as in Equation 2.1. in Laplace Domain:

$$i_0(s) = C_p s V_0(s) + \frac{V_0(s)}{R + Ls} + \frac{V_0(s)}{R_p} \qquad (2.1)$$

The coil exhibits small DC series resistance due to its specific resistivity (R). The magnetic energy dissipation due to environmental interactions is modelled by placing a resistor in parallel (R_p) with the coil inductance. The parallel capacitor (C_p) represents the electrical coupling between coil loops. i_0 and V_0 represent current and voltage applied to coil.

For PCB coil-based setups, the energy dissipation due to magnetic losses (Eddy Current-like) is negligible similar to stored electrical energy in a parallel capacitor. Concerning the given fact that the C_p has a value negligibly small whereas R_p has a very large value, Equation 2.1 can be simplified as follows:

$$i(s) = \frac{V_0(s)}{R + Ls} \qquad (2.2)$$

Concerning Equation 2.2, two parameters can be defined: ohmic loss (P_{loss}) and quality factor (or Q) of PCB coils. Ohmic loss term stands for power loss due to the parasitic resistance of copper windings of PCB coils. The resistance of PCB traces can be calculated using Equation 2.5. On the other hand, the quality factor term stands for the ratio between resistance and inductance of the PCB coil. The winding resistance appears as a resistance in series with the inductor; This is named as R_{DC} (DC resistance) or parasitic resistance. This parasitic resistance dissipates real power

in the system and dampens the system. An inductor's quality factor (or Q) is the ratio of its inductive reactance to its resistance at a given frequency and is a measure of its efficiency. The higher the Q factor of the inductor, the closer it approaches the behaviour of an ideal inductor. For resonant tank circuits, it is desirable to use higher Q-value inductors. For electromagnet quality factor can be related to power loss since higher Q means low series resistance, low power loss and lower heat generation.

$$P_{loss} = R^2 i \tag{2.3}$$

$$Q = \frac{wL}{R} \tag{2.4}$$

For calculating the parameters, the series resistance value of the coil is calculated concerning the PCB trace. PCB traces are created by chemically etched from plain copper, the chemical materials removes away the copper from top to bottom because of the chemical process, creating a copper track that has a trapezoidal shape rather than a square. If the width of traces are larger than 0.1mm then the effect of nonuniform shape is negligible. Concerning the resistivity as a function of not constant but varies with temperature change; temperature (T) and the Temperature Coefficient of Resistance (a) should be considered. The resistance of a track can then be expressed as in Equation 2.5:

$$R = (\rho \frac{L}{A})(1 + a(T - T_{ref}) \tag{2.5}$$

where T_{ref} is 20 °C, temperature coefficient of copper(a) is 4.04x10-3 K^{-1} and specific resistivity of copper(ρ) at 20 °C is 1.68x10^{8}Ω·m.

The Modified Wheeler formula [19] shown in Equation 2.6 can be used to calculate the inductance of a single-layer spiral coil. Wheeler presented several formulas for planar spiral inductors, which were intended for discrete inductors that are simple

types of radio-frequency coils. Respecting the originally published paper these formulas are correct to within 5 percent for coils with $r_{avg} > 0.2 \left(\frac{d_{out}-d_{in}}{2}\right)$.

$$L = \frac{31.33\mu_0 n^2 r_{avg}^2}{8r_{avg} + 11\left(\frac{d_{out} - d_{in}}{2}\right)} \tag{2.6}$$

The equation given above can be used to calculate the inductance of a single-layer circular spiral coil where L is inductance (H) and n is the number of turns and r_{avg} is the average radius, in meters (m), d_{out} is the outer diameter of the coil, d_{in} is the inner diameter of the coil.

For square, hexagonal, and octagonal another format of the Wheeler formula given in Equation 2.7 can be used.

$$L = \frac{K_1 \mu_0 n^2 d_{avg}}{1 + K_1 p} \tag{2.7}$$

Here, K_1 and K_2 are dimensionless coefficients that can be found in Table 2.1, p can be calculated as in Equation 2.8.

$$p = \frac{d_{in} - d_{out}}{d_{in} + d_{out}} \tag{2.8}$$

Table 2.1: Modified Wheeler formula coefficients.

Coil Types	Coefficients	
	K_1	K_2
Square	2.3	2.7
Hexagonal	2.3	3.8
Octagonal	2.2	3.5

2.1.2 Electromagnetic Theory of Magnetic Field Generated by Coils

The prime interest in coils, in terms of actuation, is their capability of inducing magnetic fields in a workspace. Therefore, two aspects should be considered in comparison: magnetic field and magnetic force.

In the most general case, the magnetic field analysis is carried out by solving Maxwell equations. In this thesis, all of the studies were held in the stationary domain with a constant current. The material of the coil trace was chosen as copper and FR4 PCB substrate was defined around the coil. Hence, the generated magnetic field H by the PCB coil can be calculated by Ampère Law as in Equation 2.9:

$$\nabla \times H = J \tag{2.9}$$

Where J is the current density (A/m^2) and it can be calculated by Ohm's Law as follows in Equation 2.10:

$$J = \sigma E + Je \tag{2.10}$$

Here, σ is the conductivity of the copper (inverse of specific resistivity), E is the electrical field and Je is the applied current density.

The given set of equations can be solved simultaneously for any defined geometry by using finite element methods. When the magnetic field is obtained, the magnetic force can be calculated as given in Equation 2.11.

$$\vec{F} = v(\vec{M}.\nabla)\vec{B} \tag{2.11}$$

Where F is a magnetic force, v is volume and M is the magnetization of permanent magnet. The magnetic flux density (B) can be calculated with the constitutive equation $B=\mu H$ for the calculated magnetic field (H). The magnetic force

calculations are carried out concerning a work plane above the PCB coil and cylindrical permanent magnet.

2.1.3 Thermal Considerations in PCB Design

IPC-2221 Generic Standard on Printed Board Design [21] accepted industry standard that defines a multitude of PCB design aspects. The requirements in the standard define certain design constraints that are intended to ensure safety, reliability, and manufacturability. The qualifications in the standard are generic standards; more specific standards applying to different types of boards are found throughout the 2220 series of standards. Some examples include design requirements regarding materials (including substrates and coating), testability, thermal management and thermal reliefs and annular rings and so on. The IPC-2221 standard is a generic printed circuit board qualification and acceptance standard for PCBs/PCBAs.

According to the IPC-2221 standard general working temperatures of PCBs are between 0 to 100 C degrees and working current below 30A. IPC-2221 provides graphs and test results at that region so that the derived formulas below are valid between these parameters. The capability of the trace to carry current is directly proportional to the cross-sectional area of the trace and temperature rise and can be calculated using Equation 2.12. In high-current applications, PCBs have high-width copper traces. Hence PCB layout design engineers need to know what trace width should be selected for a particular power circuit or device. This would increase the current carrying capacity and durability of the PCB coil.

Table 2.2: IPC-2221 pre-calculated coefficients.

Layers	Coefficients		
	k	b	c
Internal layers	0.02	0.4	0.72
External layers	0.04	0.4	0.72

$$A = \left(\frac{I}{kT_{rise}^b} \right) \left(\frac{1}{c} \right) \qquad (2.12)$$

Where A is the cross-sectional area of PCB trace, k, b and c are IPC coefficients which are given in Table 2.2, T_{rise} is the temperature rise of PCB, calculated in Equation 2.13.

$$T_{int} = T_{rise} + T_{amb} \qquad (2.13)$$

where T_{int} and T_{amb} are initial and ambient temperature respectively.

2.1.4 Fill Ratio of the Coils on PCB

Studied coil structures were used in 2D coil matrices to create linear actuators. Filling rate and layout arrangements are crucial in these type of 2D coil matrices. The maximum number of coils that can be positioned in a given space is referred to as the fill rate and can be calculated using Equation 2.13. The main goal is leaving no spaces in the work area. Although it eliminates the magnetic field gaps where the magnet can fall, it does not eliminate the asymmetrical behaviour in the direction of movement.

$$f = \frac{N}{A} \qquad (2.13)$$

Where f is the filling rate, N is the number of coils and A is the working area.

The layout design is about considering how close the coils used, how they can be placed and how the electrical connections can be made in context of expected functionality of coils. Even it is believed that the placement can be achived geometrically, this situation becomes inapplicable in practice. Some of the reasons can be counted as; the number of layers of the PCB used, the process capabilities of the PCB manufacturer and the method of the designer. There ıs no single formula or answer for this problem because it is so complex and dependent on numerous variables.

2.2 PCB Coil Design and Simulations

2.2.1 Experimental PCB Coil Designs for Actuation

In order to make simulations and tests in real world, a coil model were designed with the aforementioned design criteria. Designed coil is a two layer square coil with 15 turns. Since these designs need to be producible so that calculation and simulation can be tested and in the real application. Design parameters of the PCBs were selected following common manufacturing abilities. Currently, Standard PCB production specifications are as follows; minimum 0.15 mm thick tracks, 0.15 mm distance between tracks, 0.6/0.3 mm via diameter and hole diameter. The coils in the continuation of the study, designed to keep the cost at a minimum, taking these features into consideration coils are designed as in Table 2.3. Remaining calculations, designs and tests were carried out concerning these parameters.

Table 2.3: Coil design parameters for square planar coil

Design Parameters	Coil Type
	Square coil
Number of turns	15
Layers	2
Track With	0.25 mm
Spacing	0.15 mm
Dout	11.750 mm
Din	6 mm
Total trace length	500 mm

Following the parameters given above, planar coil was designed using kiCAD electronic design tool and commissioned for manufacturing in China. As shown in the Figure 2.2 PCB has two layers, coil is located on the top copper layer and for electrical connection to the appropriate connector bottom copper layer and through-hole vias are used so that coils have uniform shape and have no interruption. For evaluation performance of different designs, conventional methods are measuring inductance, resistance and magnetic field. Inductance and resistance were measured with an LCR meter.

15

Figure 2.2: Printed planar coil.

The series resistance and inductance of all coils have been calculated with the above-mentioned series resistance and inductance calculation formulas. To test whether the calculated values are consistent or not, which is shown in Table 2.4, PCB coils that exactly match the simulation parameters were tested. For measurements, Lutron brand LCR9184 LCR meter was used. The device datasheet values are DC resistance of 0.015 Ω and inductance of 0.15 μH in its test leads. To measure the values, the coil was connected to a connector with the ends of the bottom layer of copper. The coils were connected to the meter using the connectors and the measurement values were abtained. To minimize undesired interventions, these paths were placed as short as possible and close to each other.

Table 2.4: Calculated and measured coil parameters for various coil types.

Coil Type	Resistance		Inductance		Current Capacity
	$R_{cal}(\Omega)$	R_{mrsd} (Ω)	$L_{cal}(\mu H)$	L_{mrsd} (μH)	I_{max} (A)
Square Coil	0.98	1.08	2,38	2,04	2.65

16

Where R_{cal} is calculated resistance in ohms, R_{mrsd} is measured resistance in ohms, L_{cal} is calculated inductance in Henries, L_{mrsd} is measured inductance in Henries, I_{max} is the maximum working current of the coils.

The current capacity of the coils was calculated using Equation 2.12 and Table 2.3 These calculations were considered during design stage. Evaluating the simulation and measurements results, a critical reference of 1 A or more as operating current was picked for coils as design parameters and made an interpolation between considerable current amplitudes and coil sizes while determining these numbers and tried to select the most appropriate parameters.

2.2.2 Magnetic Field Analysis of Square Coil

Some of the common parameters when comparing coils are the magnetic field strength they generate, the dispersion and density of the magnetic field. To compare the magnetic fields generated by the coils, a series of simulations were performed, and some comparison parameters determined. These parameters are; The magnetic field norm and the magnetic field force on the horizontal axis. The simulation conditions are as follows; Coil are energized with 1 Ampere, since the magnetic field will decrease as moved away from the centre of the coil on the vertical axis, it is necessary to determine the approximate operating distance. So, this distance was picked as 1mm and the analysis refereced this distance value by analyzing Figure 2.3. In other words, the measurement magnetic field was determined as 2 mm above the coil on the vertical axis and ∓ 15 mm on the horizontal axis.

Surface: Magnetic flux density norm (mT) Arrow Surface: Magnetic flux density

(a)

Surface: Magnetic flux density norm (mT) Arrow Surface: Magnetic flux density

(b)
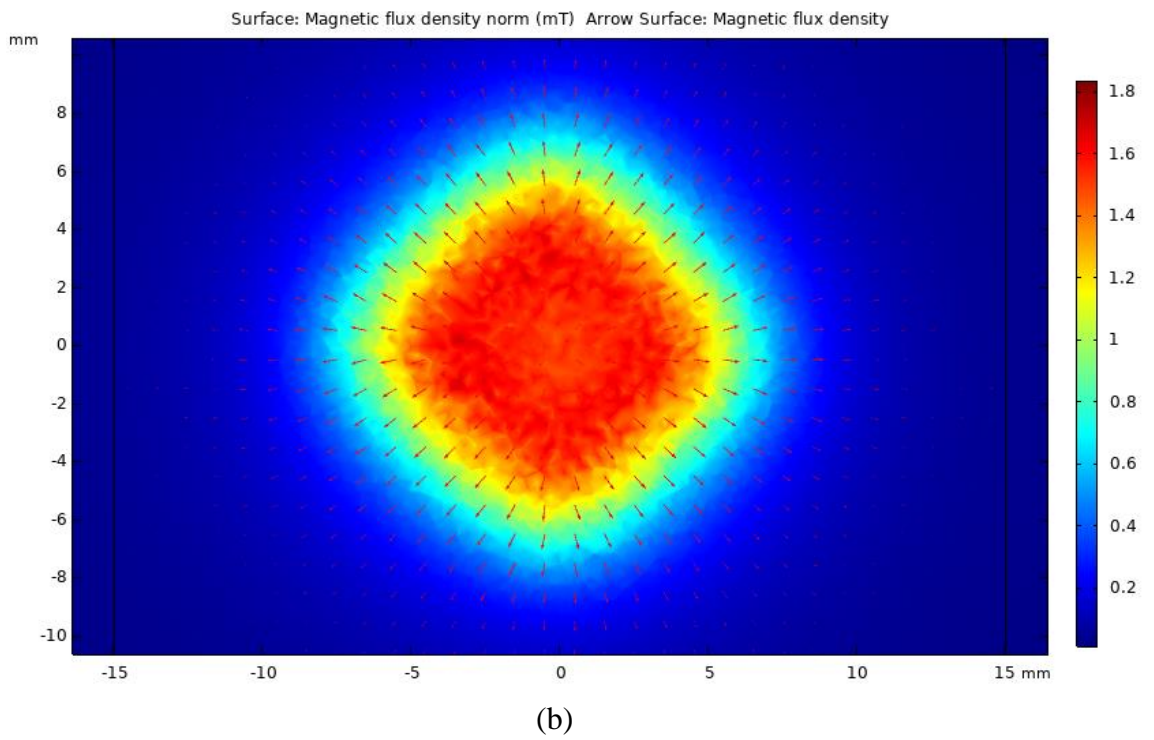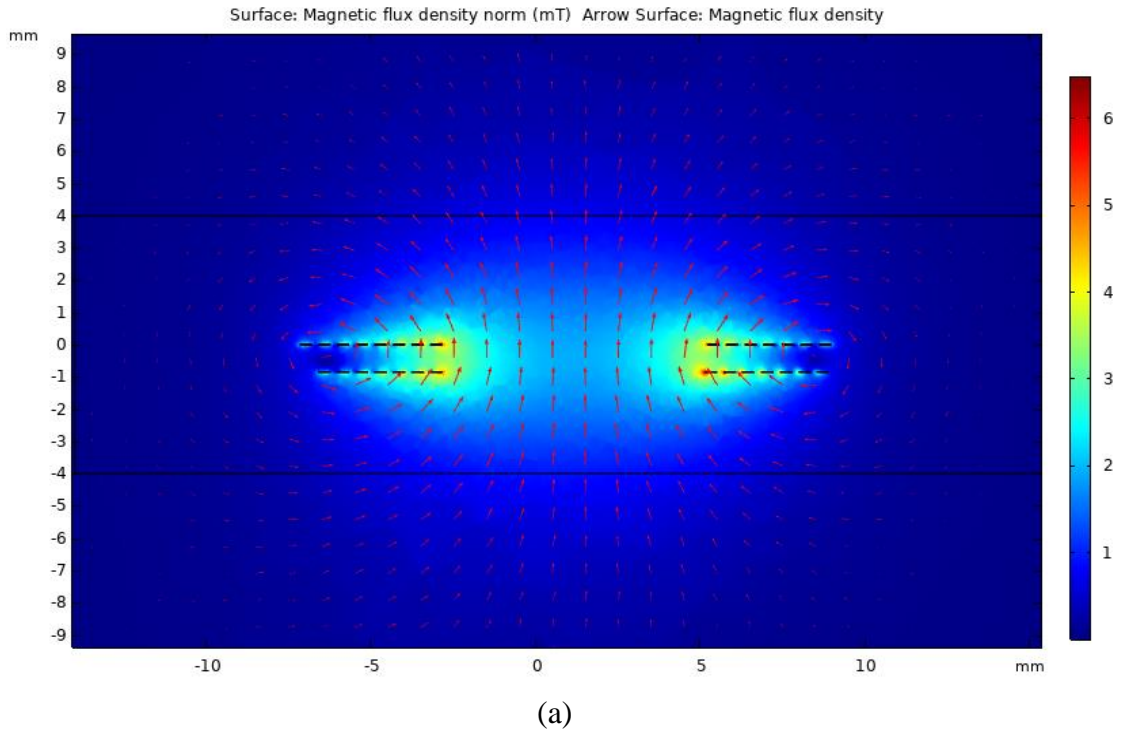
Figure 2.3: Magnetic flux density distribution in xy (a) and in xy plane (b) of the coil.
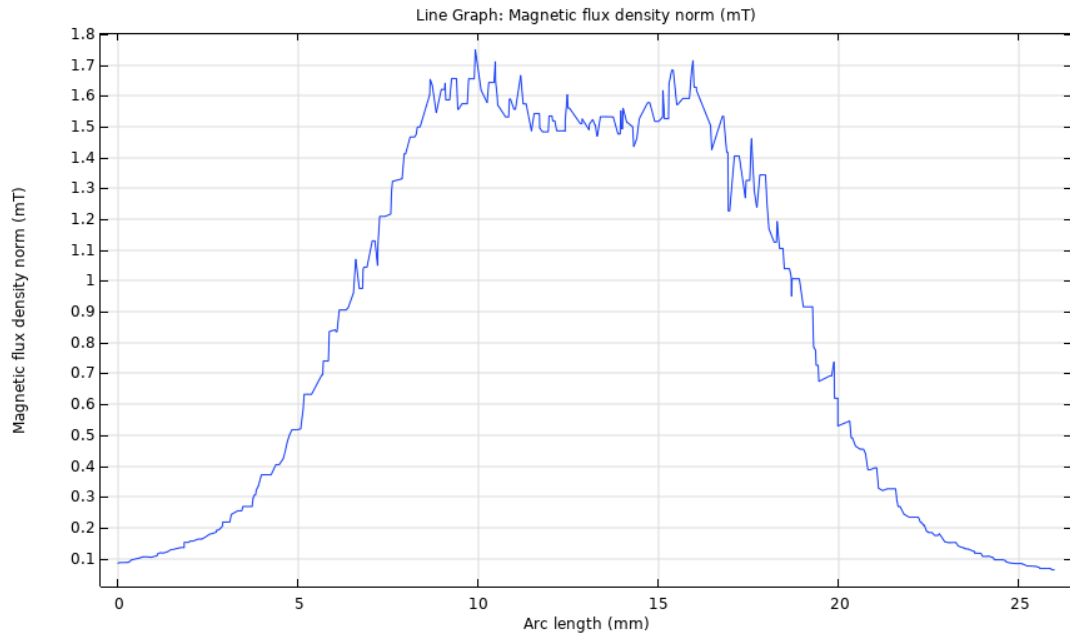
Figure 2.4: Magnetic flux density norm of the coil.

Figure 2.4. shows magnetic flux density in the x-axis of square coil. As expected, field strength reduces to zero and changes direction at the coil center, which means horizontal force will be zero at this point. To look at the homogeneity of the magnetic field produced by the PCB coils; we need to look at the magnetic field norm. As seen in Figure 2.4, the magnetic field has the shape of a bell. This is due to the fact that the coils have a coreless structure. The magnetic field increases towards the center, indicating that the magnetic force will be greater at the center than at the edges.

2.2.4 Frequency Response and Characteristic Impedance

Frequency Response describes the range of frequencies that how an individual electronic system responds to the applied frequency. Since coils are part of the system, the term of frequency response is inadequate for it so in order to express accurately impedance the term needs to be added.
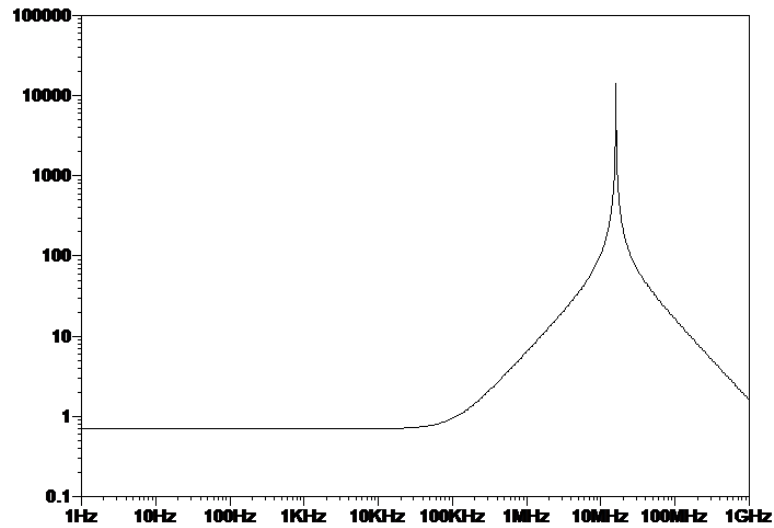
Figure 2.5: Impedance graph of the square coil

Figure 2.5 shows impedance graphs of the circular coil. In 1 Hz to 5 kHz region coil behave as a resistor, in 5kHz to 20MHz region impedance rises dramatically, in this region inductance is dominant, beyond 20Mhz parasitic capacitance is dominant so impedance is decreasing. To pass enough current to activate the electromagnet, the working frequency should be below 50kHz. Because all coils perform similarly only circular coil simulation data is shared.

Chapter 3

3. Electromagnetic Actuator Design

Within the scope of this study, the electromagnetic actuator system was designed to perform movement of the permanent magnet on a planar workspace. This gives the main motion capacity to the planar actuator. At the same time, studies have been made on the electromagnetic theory, to inspect the magnetic field that will power the movement of the microrobot. The structure of the electromagnetic actuator, coil layout and magnet structure were determined by numerical studies to be carried out based on electromagnetic theory. Following the detailed explanation of the basic structure of the system, a systematic analysis method was developed to determine the magnetic field characteristic and the structural and functional parameters of the electromagnetic system were worked out.

3.1 Steering the Magnet with PCB Coils

In order to microrobot to move from the its current position to a certain point, a structure consisting of a magnet and a magnetic core (which will be mentioned as car) on the coil must be magnetically attracted to the determined point. Microrobot locomotes indirectly by the coils. In other terms, the magnetic field generated by the car interacts with the microrobot and drags the microrobot to the desired position. The magnetic actuator design that performs the steering action is explained in detail in the following subsections.

3.1.1 Planar Coil Pattern for Actuation

A series of studies have been carried out to make an actuator with the coils whose design stages are described in Chapter 2. This subsection studies about positioning the coils. The placement of the coils on the PCB determines how and in which directions the magnet will move, as well as how much magnetic force will act on the magnet.

The first studies were carried out with the principle of placing the coils side by side in the form of a 2D array, as in Figure 3.1. The magnet placed in the centre of the target working plane, motion charecteristic is expected to act like a Cartesian system xy plane. However, tests have shown that 2D array placement tends to push the magnet over one coil rather than pull it onto the other coil. Upon this results, the studies were directed to positioning the coils in 3D array loyout.
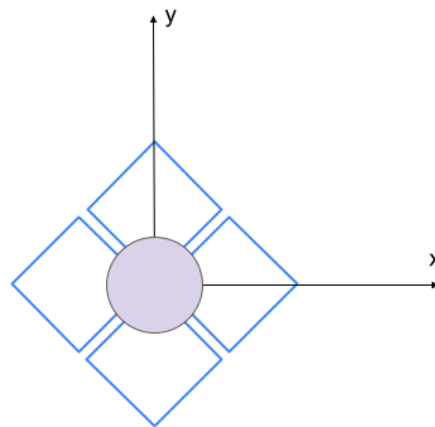
Figure 3.1: Planar actuator 2D array layout

The 3D array can be simply defined as 2D array of coils stacked on top of each other. As shown in Figure 3.2, the coils in the upper layer are arranged side by side in a planar fashion. The coils in the back layer are offset in the x-axis by half the width of the coil. The main purpose of this arrangement is to overlap the surface with at least two coils in the direction of the targeted movement of the magnet. Thus, when the coil is energized, it is guaranteed to be pulled by the coil instead of being pushed.
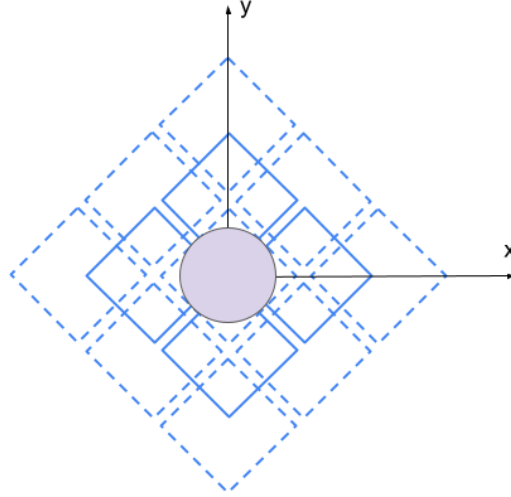
Figure 3.2: Planar actuator 3D array layout

3.1.2 Electromagnetic Theory to Realize Magnet Steering

The magnet, directed in a certain direction by the magnetic pole formed by the electromagnet energized in the direction of motion, performs linear motion along the motion axis with the effect of a uniformly varying magnetic field over a certain magnitude, in the same direction as the magnet magnetization vector. To provide the linear force to move the magnet, the controlled change in magnetic flux density must be uniform and large enough to overcome the friction force between the magnet and the movement surface.

Under a uniformly changing magnetic field, the magnetic repulsion force to act on the magnet with the magnetization vector M, can be calculated using Equation 3.1 and can be expressed mathematically:

$$\vec{F}_m \ = \ V \, (\vec{M} \cdot \nabla)\vec{B}_D \qquad\qquad (3.1)$$

$\vec{M}$ Magnetization vector of the microrobot, V represents the volume of the microrobot. $\vec{B}_D$ is the smooth changing magnetic flux density which expressed in Equation 3.2.

$$\vec{B}_D = \mu_0 \mu_r \vec{H}_D \qquad (3.2)$$

μ_0 is the magnetic permeability of the air, μ_r is the magnetic permeability of the magnet, $\vec{H}_D$ stands for uniformly varying magnetic field vectors.

By combining the formulas defined above and performing the necessary mathematical operations, we can find the magnetic force acting on the magnet in which direction and size with Equation 3.3.

$$\begin{bmatrix} F_X \\ F_Y \\ F_Z \end{bmatrix} = V. \begin{bmatrix} M_X \cdot \dfrac{\partial B_X}{\partial X} & M_Y \cdot \dfrac{\partial B_Y}{\partial X} & M_Z \cdot \dfrac{\partial B_Z}{\partial X} \\ M_X \cdot \dfrac{\partial B_X}{\partial Y} & M_Y \cdot \dfrac{\partial B_Y}{\partial Y} & M_Z \cdot \dfrac{\partial B_Z}{\partial Y} \\ M_X \cdot \dfrac{\partial B_X}{\partial Z} & M_Y \cdot \dfrac{\partial B_Y}{\partial Z} & M_Z \cdot \dfrac{\partial B_Z}{\partial Z} \end{bmatrix} \qquad (3.3)$$

2.3.3 Magnetic Force Simulation Between Coil and Magnet

To study magnetic force acting on a Neodymium permanent magnet, a simulation setup was designed as shown in Figure 3.3. and Figure 3.4.
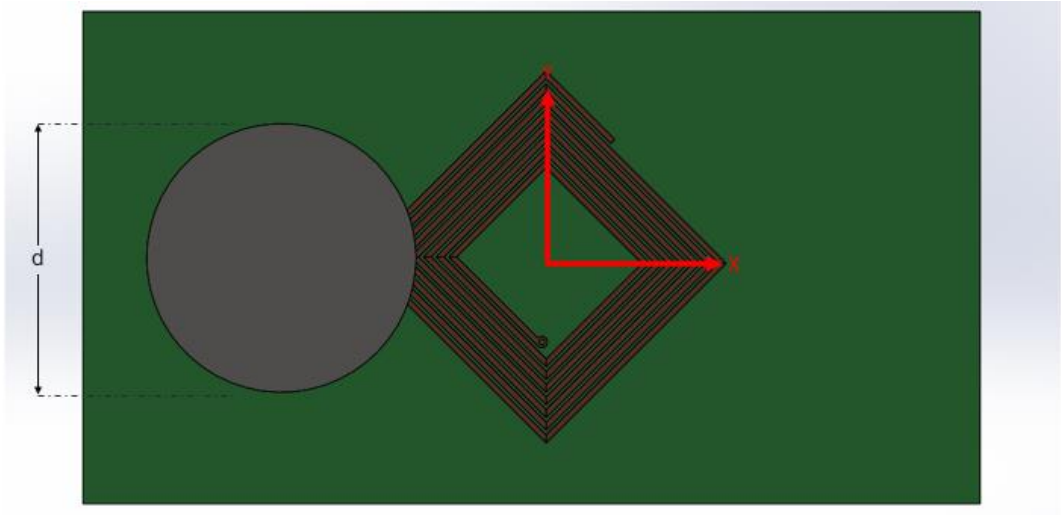
Figure 3.3: Magnetic force simulation setup top view
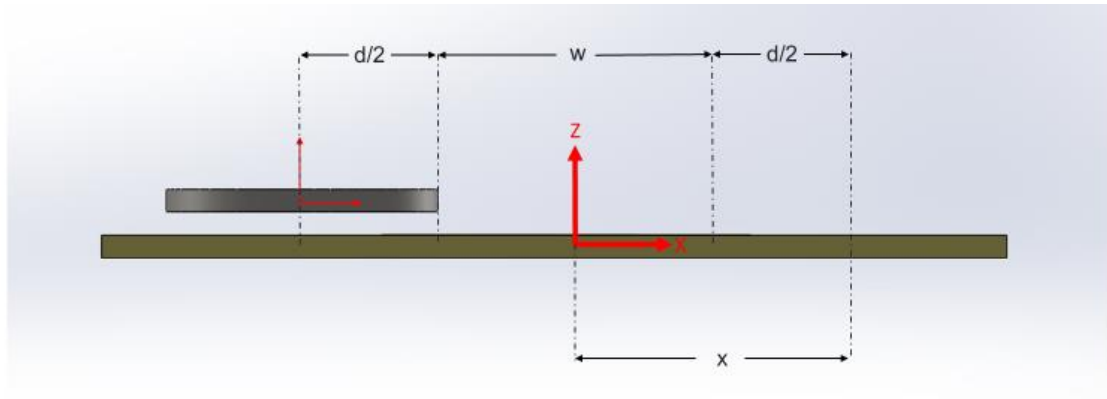
Figure 3.4: Magnetic force simulation setup side view

A series of simulations were run to see the effect of the magnetic field produced by the coil on a magnetic particle or a magnet. The simulation parameters are as follows; The coil is energized with 1 A DC current, the magnet is 12 mm in diameter and 2 mm thick and made of N35 material. The magnet moves on the coil above 1mm in the vertical axis and ∓15 on the horizontal axis. Thus, at any point of the 30 mm direction, it is determined how much magnetic force is applied to the magnet. The reason why the magnet was chosen as 12 mm can be explained as follows: When two coils are positioned side by side (a and b), the distance between their centers is on average 10 mm, although the coils differ in their designs. This measure shows that when a coil is energized, the magnet affected by the magnetic field will be attracted towards the center (if the poles are polarized) and will reaches equilibrium point at the center. If the magnet is to be moved from coil A to coil B and the magnet diameter is smaller than the coil diameter, it cannot be moved as it will be out of the effective magnetic field, as seen in the magnetic field graphs Figure 2.4. To summarize, smulations results show that the effective way to control the magnet in the setup is that the diameter of the permanent magnet should be approximately equal to the coil diameters.
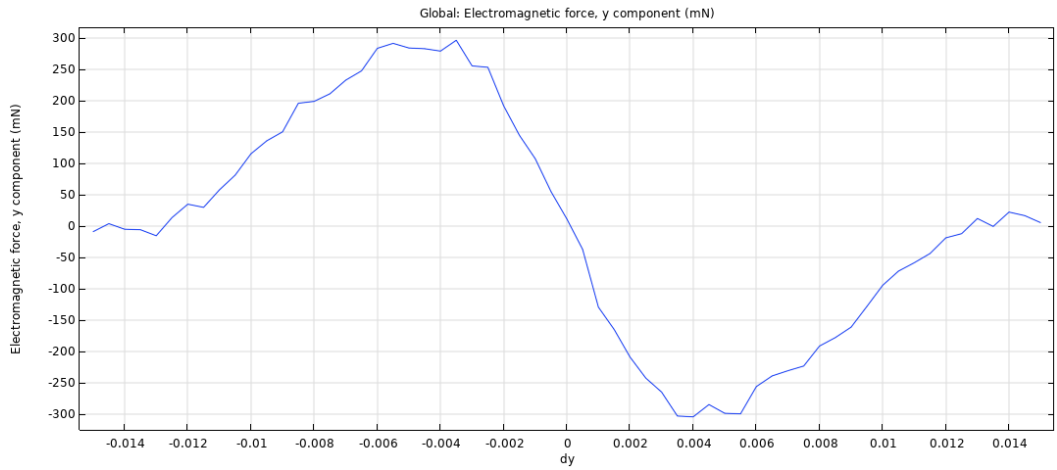
(a)
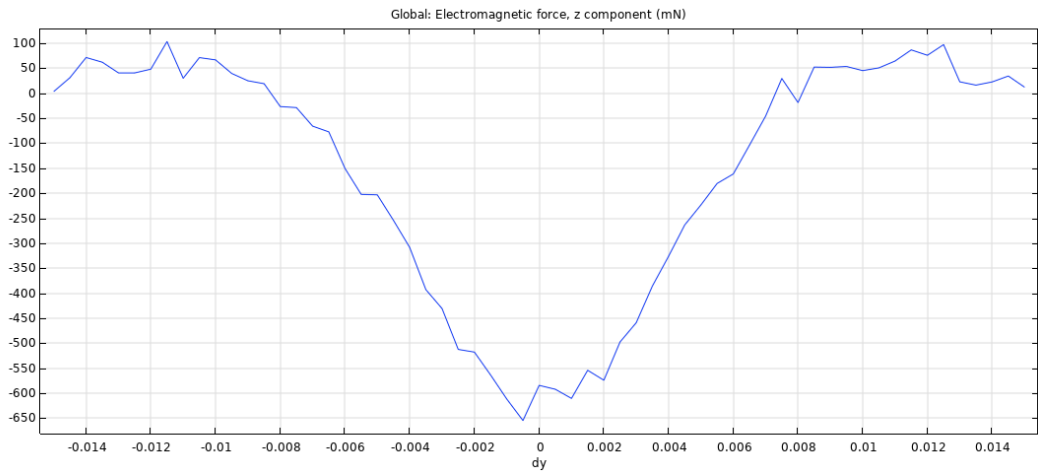
(b)

Figure 3.5: Magnetic force on a 12x2 mm circular N35 magnet of the square coil, on y direction (a), on z direction (b)

Due to PCB coils having very few turns and aperating relatively low current values, they generate lower magnetic field strengths than conventional electromagnets on the market. Moreover, since they do not have a magnetic core, the generated magnetic field has a bell-shaped profile.

The proposed system goal is to move the permanent magnets on a 2D surface with the help of these coils. The point to be considered in such applications is that the friction force should be smaller than the pulling force. The direction of the force applied by the PCB coils to the magnet passes from the horizontal axis to the vertical

axis as it approaches the center. Due to this structure of electromagnets, the friction force increases as the magnet gets closer to the center.

3.3 Steering the Microrobot with PCB Actuator

PCB-based electromagnetic actuator uses a specific end effector that interacts with the microrobot and locomotes it. The part of magnetic actuator design that performs the steering of the microrobot is explained in detail in the following subsections.

3.3.1 Characteristics of the Microrobot Intended to Move

In this thesis, it is aimed to use a spherical particle as a micro robot. The surface of this spherical particle is expected to be fairly uniform, and the diameter is the same from all angles so that it can move uniformly in all directions when a magnetic force is applied. In addition, since this microrobot shall move on a lubricant, its surface must be smooth so that there is not too much drag force while moving and it does not get stuck on the surface bulges. Concerning the given requirements, it was concluded that this type of spherical particle cannot be manufactured in a general-purpose laboratory environment without industrial equipment.

Figure 3.6: Micro robot and dimension

After some market investigation, the balls in the ball bearings are one of the most suitable spherical particle solution for the task. These balls have almost perfect spherical geometry and great finishing surface due to their working environment and principles. Since small-scaled spheres are needed for micro work, miniature bearings with a diameter of 4~5 mm were picked, then disassembled and the balls inside were taken with measured diameters; 1.95mm, 1.55mm (seen in Figure 3.6), 0.79mm, 0.65mm. The small size of the spheres increases the compatibility for the targeted micro manipulation, whereas it makes it difficult to move the spheres with the magnet under them. The experiments showed that the spheres with a diameter of less than 1.55 mm have weaker interaction with magnets. Hence, sphere ball with the diameter of 1.55 mm was chosen for the micro robot and properties shown in Table3.1.

Table. 3.1: Properties of micro robot

Diameter	Alloy	Average Relative Permeability	Drag Coefficient (C_d)
15 mm	C440	1000	0.5

3.3.1 Magnetic Theory to Realize Microrobot Steering

When a magnetic particle is subjected to a magnetic field, it experiences a magnetic force. This force arises due to the interaction between the magnetic field and the magnetic properties of the particle. The magnetic force acting on a magnetic particle can be expressed in Equation 3.4, which states that the force is proportional to the magnetic field strength and the magnetic moment of the particle. The magnetic force acting on a magnetic particle depends on various factors. Firstly, the strength and direction of the magnetic field play a crucial role. The magnetic field exerts a force on the particle, either attracting or repelling it, depending on the orientation of the magnetic moments. Secondly, the size, shape, and magnetic properties of the particle influence the magnitude of the force. Larger particles generally experience stronger forces, while the shape and alignment of the magnetic moments affect the direction of the force.

In the non-uniform magnetic field, there will be a force acting on the magnetic particles[22], force can be calculated using Equaion 3.4.

$$\vec{F} = \frac{V \cdot \chi_p}{\mu_0} (\vec{B} \cdot \nabla)\vec{B} \tag{3.4}$$

Where $\vec{B}$ is the magnetic flux density can be expressed in Equation 3.5, V is the volume of the particle, χ_p is the magnetic susceptibility of the particle, μ_0 is the permeability of free space, $\vec{M}$ is the magnetization of the fluid and $\vec{H}$ is the external magnetic field strength.

$$\vec{B} = \mu_0(\vec{M} + \vec{H}) \qquad (3.5)$$

3.3.2 Magnetic Analysis of Car and Magnetic Force on Microrobot

The ferromagnetic core design is designed according to the dimensions of the micro robot. The dimensions of the particle micro robots intended to be used vary between 0.79 mm and 1.55 mm. In the targeted movement mechanics, the car and the micro robot must be magnetically locked. In order to achieve this, the magnetic field lines must be compressed to an area equal to the cross-sectional area of the micro robot. This is exactly what the ferromagnetic core does. It condenses the magnetic field produced by the permanent magnet into a channel. Thus, the micro robot can be moved in a more precise way. In cases where the dimensions of the micro robot and the core do not match, the dead zone occurs too much in the robot movement that magnetic locking does not occur.
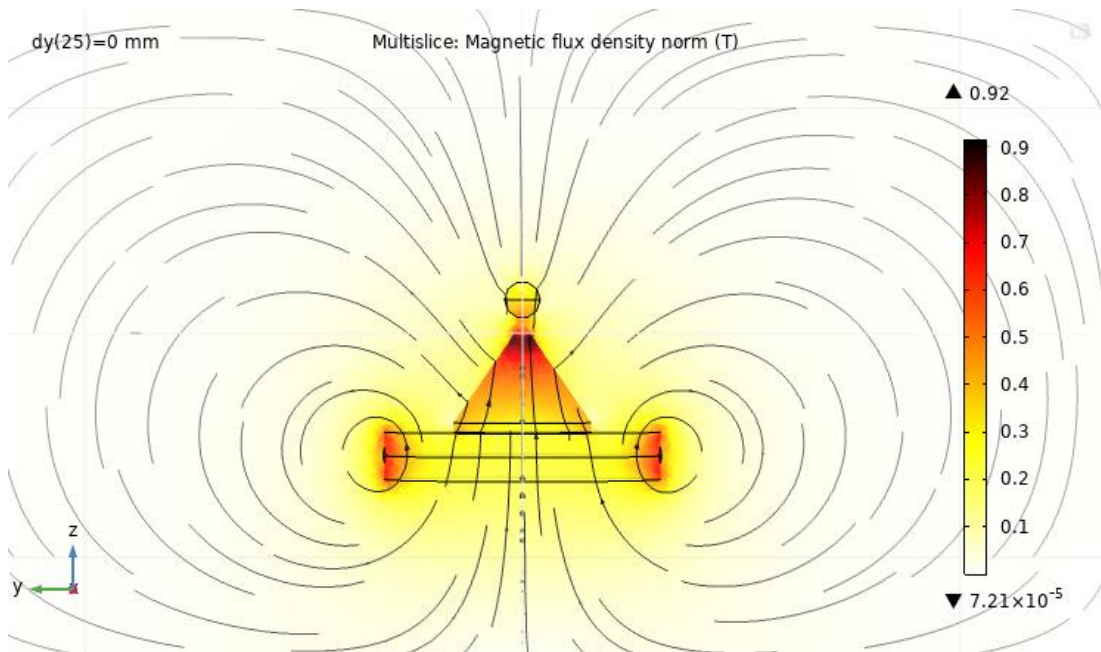
Figure 3.7: Magnetic flux density distribution in YZ plane

in FEM simulation given in Figure 3.7, can be seen that the core concentrates the magnetic field in a narrow channel. In Figure 3.8, the related force graphs the 1.55

mm ball exerts on the y and z axes are given. The simulation was carried out in the following manner. The car consisting of a magnet and core (it was not added to the simulation since the carcass is made of plastic, it was not added to the simulation because it would not make a magnetic difference) was kept fixed and was carried out by moving microrobot between -13mm and 13mm in the y-axis and kept fixed 1mm in the z-axis.
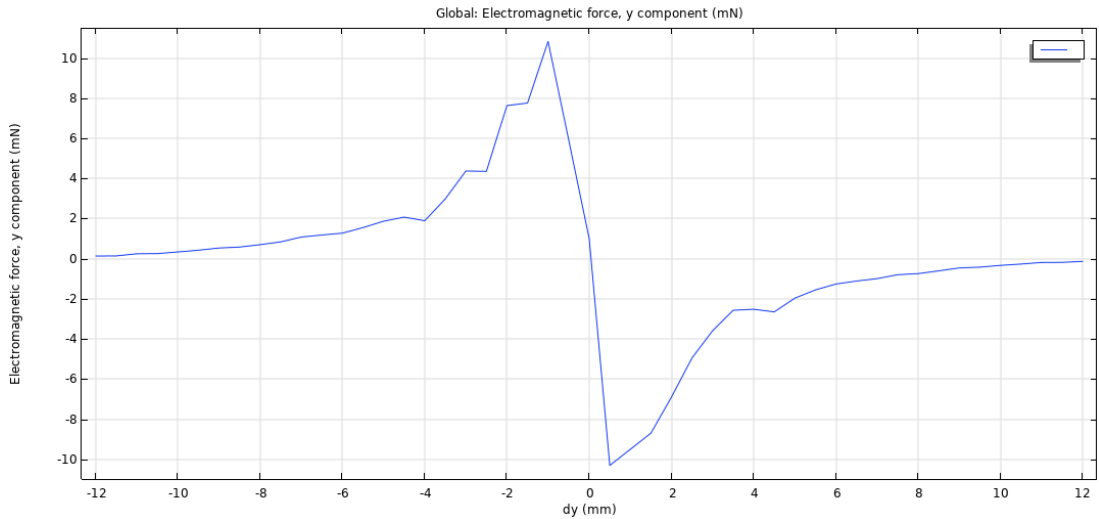
(a)
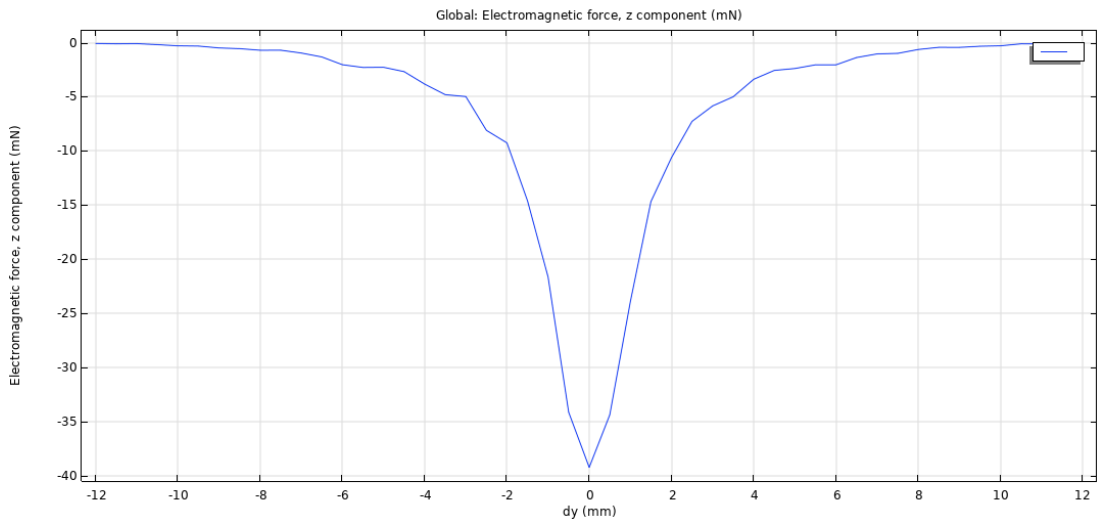
(b)

Figure 3.8: Magnetic force on 1.55mm ball, on y direction (a), on z direction (b)

The results show that, as the ball approaches the center of the core, the force increases on the y-axis and changes direction at the very center. This means that the ball is pulled towards the center regardless of position and tries to bring the ball to the equilibrium position where the net force is zero. When the force on the axis is examined, the force acting on the ball approaching the center increases, just like on the y-axis. However, it does not change direction as it does on the y-axis. The coil continuously provides a downward pulling force in the z-axis to the ball. As a result, an undesirable situation occurs. The pulling force in the Z axis increases the friction between the micro robot and the motion surface.

3.3 Drag Calculation of Microrobot in Lubricant Oil

When a sphere particle moves through an oil medium, it experiences drag force, which opposes its motion. The magnitude of this drag force depends on several factors, including the size and shape of the sphere, the properties of the oil, and the velocity of the particle. The drag force acting on a sphere in oil is typically described by Stokes' Law, which applies to small particles moving at low Reynolds numbers. According to Stokes' Law, the drag force is directly proportional to the velocity of the sphere and the oil's dynamic viscosity, and it is inversely proportional to the radius of the sphere. The relationship between the drag force and the velocity is linear until the particle reaches its terminal velocity, at which point the drag force balances the gravitational force acting on the sphere. Understanding the sphere particle drag force in oil is crucial for predicting the behaviour of particles in various processes, optimizing oil-based systems, and designing efficient separation techniques. Force acting on sphere microrobot expressed in equation 3.6.

$$F_d = C_d \times 0.5 \times rh \times Vel^2 \times A \qquad (3.6)$$

Where F_d is equal to the drag force, rh is the density, Vel is the velocity, A is a reference area, and C_d is the drag coefficient. The density of sunflower oil is 918.8 Kg/m^3

The reference area can be calculated as the frontal area of a sphere using Equation 3.7,

$$A = \frac{\pi \times d^2}{4} \qquad (3.7)$$

With these calculations drag force acting on micro robot can calculated. Especially in high speeds drag force needs to be considered. It can directly infuliences commutation times of the coils. If coils commutate higher than max speed that micro robot, micro robot may not get rid of magnetic locking and go to target position.

Chapter 4

4. Hardware Design and Production

4.1 Electronic Hardware Design and Production

The electronic hardware content of the PCB-based electromagnetic actuator includes systems designed to control the functional parameters that enable the movement of the microrobot in the plane. It can be divided to 6 sub-subsystem headings: driver board, actuator board, modular coil boards, microcontroller board, heatsink/damper PCB plates and power supply and explained in detail in the following sections.

4.1.1   Modular Coil Boards for PCB Planar Actuator

In the design of PCB actuators, modular PCBs were manufactured using planar PCB coils designed in Chapter 2. These PCBs are 13.35x12.20 mm in size and the coil size in the PCB is 12x11.5 mm. There are copper holes (castellated holes) used as solder pads in the shape of a half-moon on both sides of the coils. Thanks to these pads, modular coils can be soldered to the carrier board like an SMD component. The main reasons for making the coils modular can be listed as follows; It is based on the idea of arranging the coils on the PCB as a standard component, instead of drawing the coils one by one, in a situation where more than one actuator needs to be designed first. The main reason was to shorten the time spent while designing the actuator. The second reason was that, there is about four times the price difference between a two-layer PCB and a four-layer PCB. This cost increases exponentially as the copper solid increases. Therefore, all PCBs were designed with two copper layers in order to reduce the cost while the design is produced, thus reducing the cost.
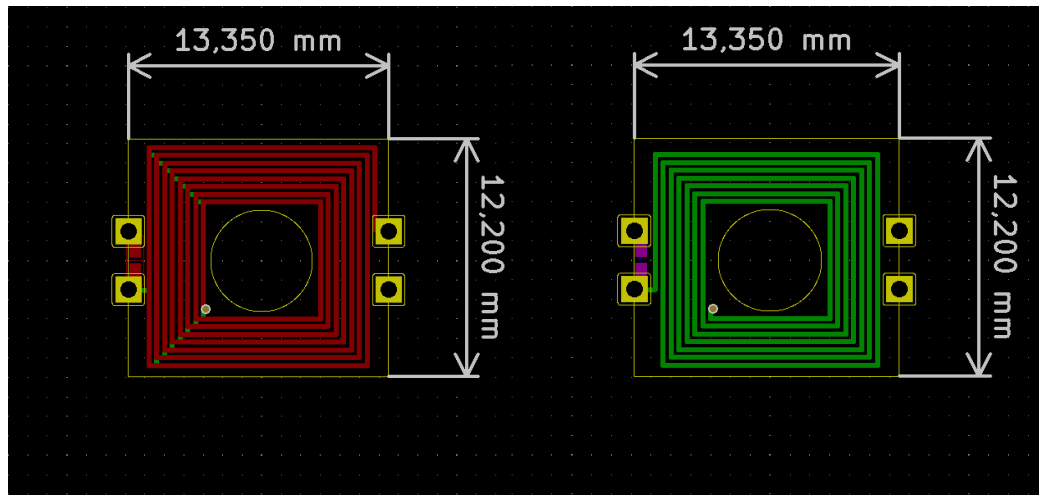
(a)   (b)

Figure. 4.1: Modular coil board (a) front copper, (b) back copper windings

The coil design is shown in Figure 4.1 and panalized/manufactured version can be seen in Figure 4.2. The design follows the specifications in Table 2.3. The design parameters of the PCB were chosen taking into account today's standard manufacturing capabilities. Standard PCB production features are as follows; tracks with a minimum thickness of 0.25 mm, distance of 0.25 mm between tracks, pad diameter of 0.6/0.3 mm and hole diameter. Designing PCBs with the common manufacturing features is very important in terms of cost. While reducing the dimensions does not affect the manufacturability much, they increase the cost considerably.
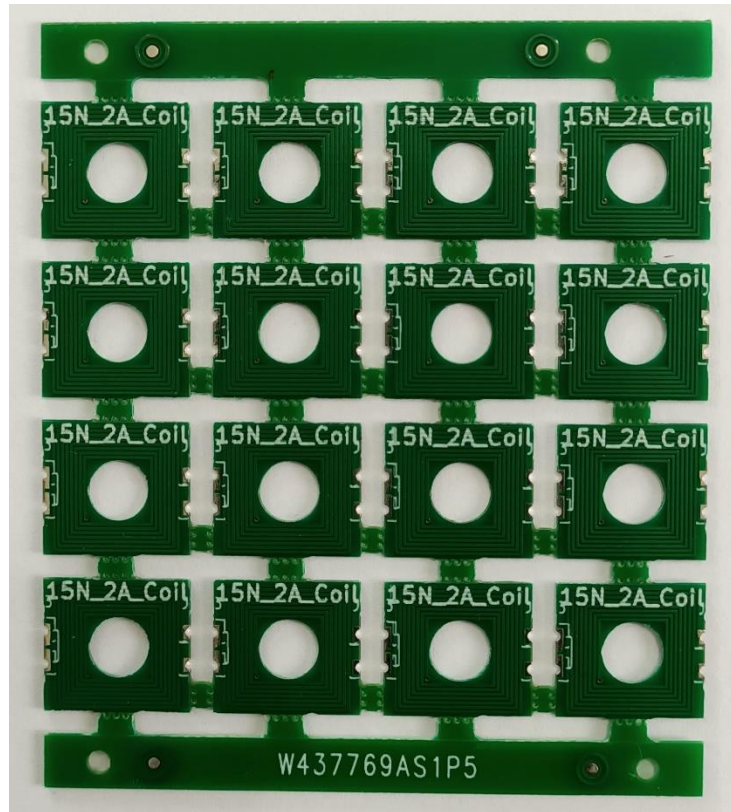
Figure 4.2: Panelized and single modular coil boards

4.1.2   PCB Actuator Carrier Board for Coil Assembly

The actuator board was designed so that the modular coils can be assembled into an array and connected to the driver board. Carrier Board is 100 x 100 mm in size, which PCB manufacturers in the market recommend and provide a low production price for the low cost of the system.
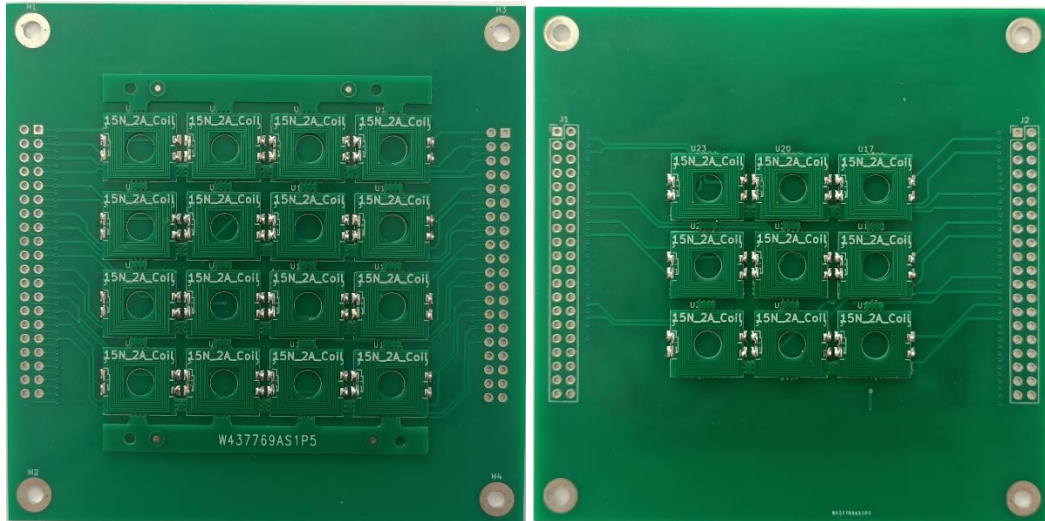
(b)	(c)

Figure 4.3: PCB Actuator Carrier Board assembled version front (a) and back (b) side

There are 16 coils in the form of a 4x4 arrangement can be seen in Figure 4.3, on the top layer of the PCB, and 9 coils in the form of 3x3, on the bottom layer of the PCB, coming to the diagonal centers of the coils on the upper layer. The carrier board has two layers and with thickness of 0.8 mm. There are pads that can be soldered on both sides of the PCB, and the electrical connections of the coils go from these pads to the 2x20 pin connectors on both sides of the PCB. The connectors were intentionally positioned as far away from the working space as possible, to prevent the nickel in the connector pins from affecting the magnet.

4.1.3   PCB Actuator Coil Driver Board

Each coil need a separate power circuit in the system. There are ready-to-use H-bridge and single-mosfet motor driver circuits are most common components in the market for use in such tasks, however, these components increase the cost of the system incredibly, considering that it costs 5 to 10 dollars per coil and there are 25 coils in the system. Also, these components shall cause a big cable mess during integration into the system, as they are designed for different requirements, and they will prevent the system from having a modular/compact structure. For these reasons, the need to design a driver board has arisen.

For the driver board design, the use of motor driver ICs from electronic manufacturers was considered first. However, it has been understood that the operating currents and voltages of these driver ICs are not suitable for the system planned to be used. For this reason, it was decided to design a driver circuit from discrete electronic elements. If the design criteria are listed; In order to be compact and small to be designed, all electronic elements to be used have been chosen as surface mount technology, MOSFET transistors to carry current, and BJT transistors have been chosen as small signal switches.
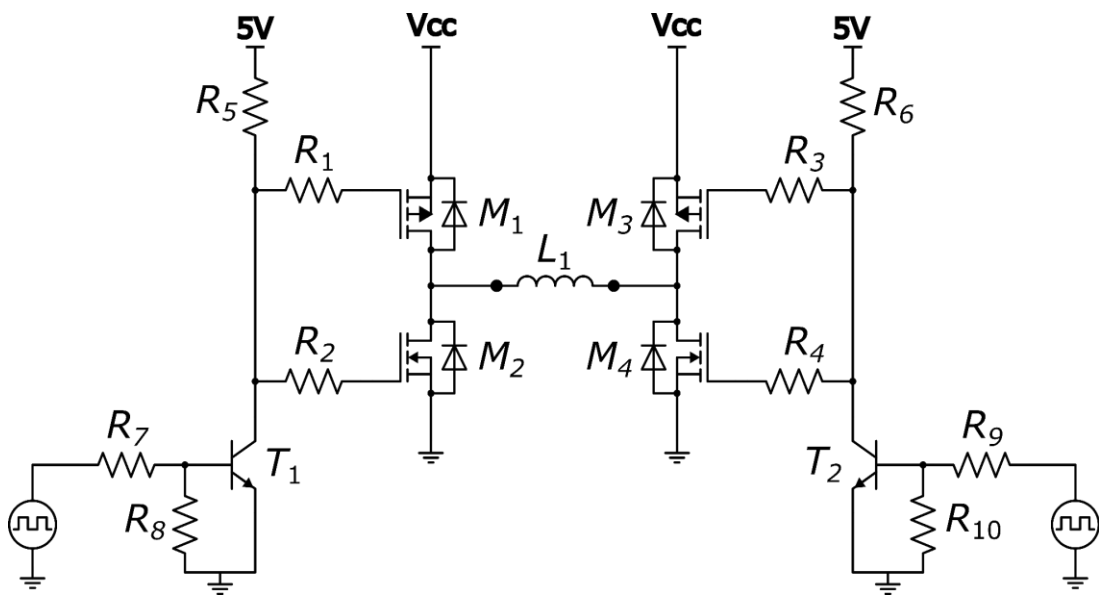
Figure 4.4: H-Bridge driver circuit

First, the H-bridge circuit was designed from discrete electronic components to replace the H-bridge IC, shown in Figure 4.4. This circuit was designed with the principle of 2-state operation in order to have as few components as possible. The 2-state principle is that the outputs of the circuit to be connected to the coils have two different states. The reason for this is that P-channel MOSFET is used as a high-side switching element and N-channel MOSFET is used as a low-side switching element to reduce the number of components to be used in the circuit. Depending on the PWM inputs in the circuit, two switches remain open and two switches remain closed.
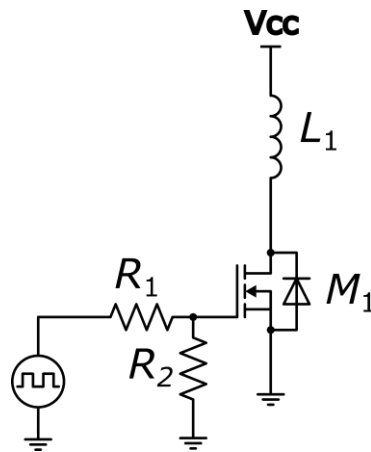
Figure 4.5: Low-side driver circuit

In the tests carried out, it was seen that the permanent magnet can be moved without the need for double-sided energizing of the actuator coils. On top of that, a low-side driver circuit was designed to reduce system complexity and cost. In this circuit shown in Figure 4.5 and Figure 4.6, one terminal of the actuator coil is connected to the supply voltage and the other terminal is connected to an N-channel MOSFET. This MOSFET turns on and off with the signals it receives from the microcontroller board. Thus, a movement mechanism based only on the pulling force is formed between the actuating coil and the permanent magnet. Also, this circuit supports PWM modulation like the other circuit.
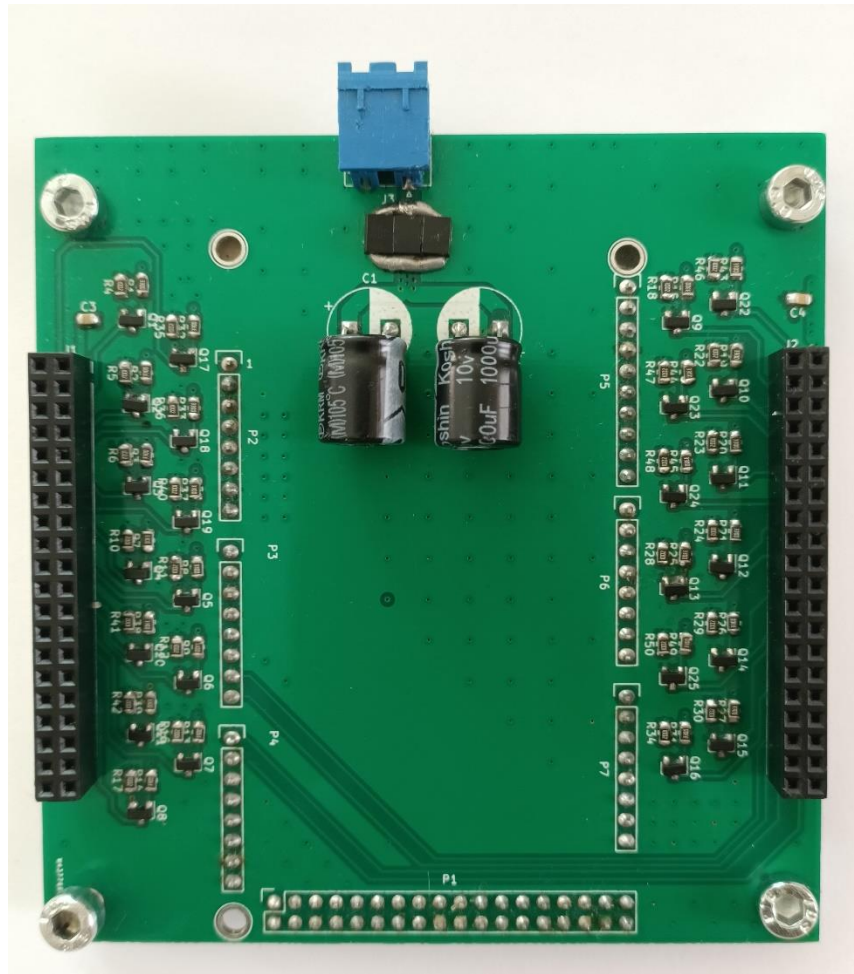
Figure 4.6: Low-side driver board.

4.1.4　Heatsink/Damper/Spacer PCB Plates for PCB Actuator

The actuator surface is shown in Figure 4.3. After the modular PCB coils are soldered onto the actuator board. In order for the car to move on the actuator surface, the coils must be 1 mm above and the movement surface must have a smooth structure. In addition, the coils used as electromagnets make their power consumption on the series equivalent resistance under DC energizing, and as a result, the PCB activator coils heat up as a thermal center. In an uncontrolled environment, this may cause the PCB laminates to overheat and burn, and when it exceeds 100 degrees, the Neodymium permanent magnet in the car loses its magnetic field, and eventually the PCB actuator may malfunction due to these reasons. In order to

overcome these problems, 2-layer PCBs were designed to function as a heatsink and damper that are thin enough to fit into the existing very narrow volume.

Figure 4.7: Heatsink/Damper/Spacer PCB Plates

The designed PCBs are 0.8 mm thick and there is a 35 µm thick continuous copper sheet on both sides. In order to increase thermal mass and conduction, the coppers in the lower and upper layers are electrically connected with through-hole vias with a hole diameter of 0.4 mm for every 5 mm interval. The vias have a hole diameter of 0.4 mm and after drilling, electrolysis chemical treatment is applied to coat the inner surfaces of the vias; where $Cu2+$ takes electrons and becomes elemental copper and is plated over the drilled holes. The thickness of the coated copper is generally between 20~30 µm. Since vias cause a bump of a few micrometers on the surface, PCBs without vias were designed and produced for use in experimental studies. As a result of experimental studies, it was seen that the increase in friction caused by vias can be ignored.

Another feature of these PCBs is that they dampen the oscillations caused by the car coming to a rapid stop at high speeds. The reason for the damping is that due to the changing magnetic field while the magnet is moving, eddy currents are formed in the copper plate and create a reaction force in the opposite direction of the movement of

the magnet. As the movement speed of the magnet increases, the rate of change in the magnetic field also increases. If the oscillation rate of the magnet is high and in this case, the eddy currents induced to the copper are also high, so in this case the reaction force applied to the magnet is also high. Power loss due to eddy currents can be calculated using Equation 4.1.

$$P_{eddy} = \sum_{i=1}^{h} B_{peak}(i)^2 (if)^2 \, \sigma \, w_{cu}^2 V_{copper} \qquad (4.1)$$

Where P_{eddy} is the total power loss of eddy currents, i is the order of harmonics, B_{peak} is the peak of each harmonic of the magnetic flux density, f is the fundamental frequency, σ is the conductivity of the copper, w_{cu} is the copper trace width, and V_{copper} is the total copper volume inside of the stator.

4.1.5   Power Supply and Wiring for Operating PCB Actuator

The system needs 3 different power supplies to operate. The voltages needed are; 5V, 9V fixed voltages and 3V-5V regulated power supply. The 5V power supply is the voltage required for the microcontroller to perform its functions and reaches the microcontroller board by the computer via USB connection. The 9V power supply uses the workspace as the power supply for the LEDs used for lighting and comes from the 9V 0.6A wall adapter. 3V-5V adjustable voltage is used to energize the coils on the actuator and the Unit UTP1310 is fed by 32V 10A adjustable DC power supply, shown in Figure 4.8.

Figure 4.8: Unit UTP1310 32V 10A adjustable DC power supply

Since the coils used in the actuator design have a series equivalent resistance of 1 Ω and the MOSFETs used as the switching element, they draw a current of around 3A when 3V applied. Since more than one coil can be energized at the same time in the system, the peak current consumption increases in multiples of three amps. The points to be considered here are; The power supply must be able to provide sufficient current and the impedance of the energy-carrying cables between the power source and the actuator must be low. In cases where the power cables are thinner than they should be and have high current consumption, there is more voltage drop on the cable than the system can tolerate. Therefore, when the coils are energized at the same time, the coils pass a lower current and give a lower magnetic field compared to their single energizing.

4.1.6   Microcontroller Board for Controlling PCB Actuator

A microcontroller was used to control the switching elements in the system according to the commands received from the computer. The switching frequency in the system is relatively low. In the experiments, the system does not respond to

pulses above 300 Hz. Therefore, the PWM frequency did not need to be high. Another feature is that this microcontroller must have at least 25 digital outputs. Because each actuating coil has a MOSFET defined for itself and these MOSFETs need to be controlled separately. And also, this microcontroller board should have a common, cheap and modular structure. For these reasons, Arduino MEGA , shown in Figure 4.9, was chosen.
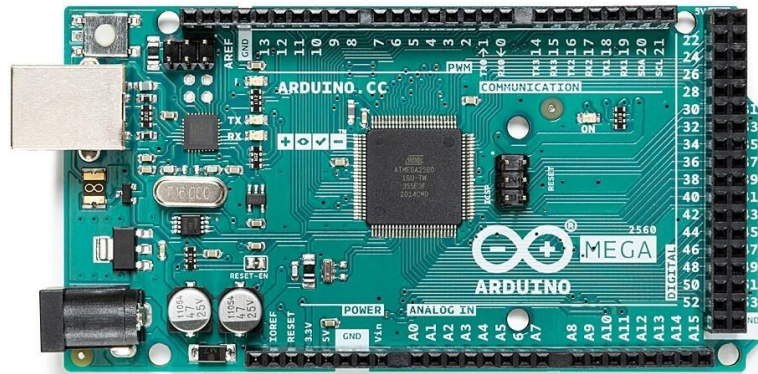
Figure 4.9: Arduino MEGA

4.2 Mechanic Hardware Design and Production

4.2.1   Car Design

In this study, the term "Car" is referred as the structure consisting of a magnet, a ferromagnetic core and a carcass that holds them together, given in Figure 4.10. The components of the Car can be explained as follows; magnets interact with the magnetic field produced by the coils to exert a repulsive and attractive force on the structure that needs to be moved, the ferromagnetic core concentrates the magnetic field produced by these permanent magnets towards a narrow field, increasing the

interaction of the ball load in the working space with the magnetic field, the carcass keeps these two particles together.
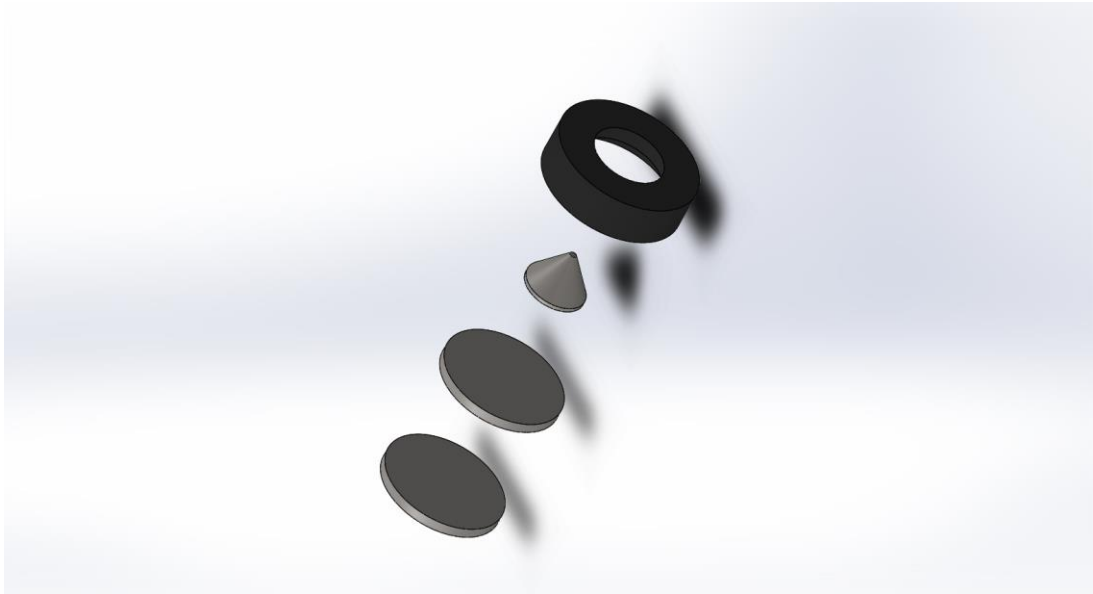
Figure 4.10: Car assembly

In the tests and simulations, it was observed that placing two N35 magnets of 12 mm in diameter and 1 mm in height on top of each other increases the force applied by the coils to the magnets and increases the mobility of the magnets. Eventually, in the Car design , two magnets were used .

4.2.2   Electronic Board Stack

The designed and ready-to-use cards are modularly designed or supplied on top of each other. PCB assembly is combined with sandwich assembly logic.

Figure 4.11: PCB assembly

As seen in Figure 4.11. The assembly consists of 7 different parts. These are; one Arduino MEGA microcontroller board, one 25 channel coil driver board, two heatsink/spacer boards, 1 carrier board, 25 modular coil boards and a cardboard cut in coil size. The electrical connections between the layers are provided by pin headers with 2.54 mm pitch. These connectors leave enough space between the PCBs and are very suitable for signal and 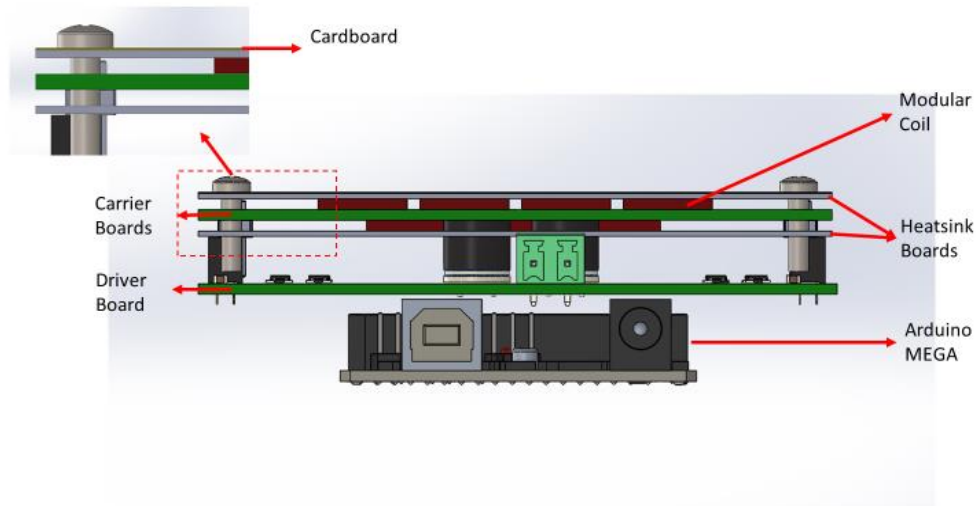power transmission. Coil carrier, coil card, heatsink and cardboard subassembly are made with holes in the four corners and 4 plastic M3 bolts.

4.2.3   System Assembly

Figure 4.112. shows the projected assembly of the system. The system consists of 5 sub-assemblies; The chassis, the camera and its holder, the trolley, the PCB sandwich and the workspace. In the chassis, 20x20 extrusion profiles were used to form the skeleton of the system. These profiles are connected to each other from several points with in-duct mounting apparatus. Afterwards, the PCB assembly was mounted to the profiles with 4.2 mm diameter holes on the driver board and nuts for M4 bolts/channels. The profile that stands perpendicular to the PCB mounting is placed to hold the camera. A smart phone was used as a camera. The intended use of the smart phone is due to the low-budget cameras that do not see the small-sized

46

microrobot and the low video shooting speeds. The phone is held by two plastic apparatus on the profile.
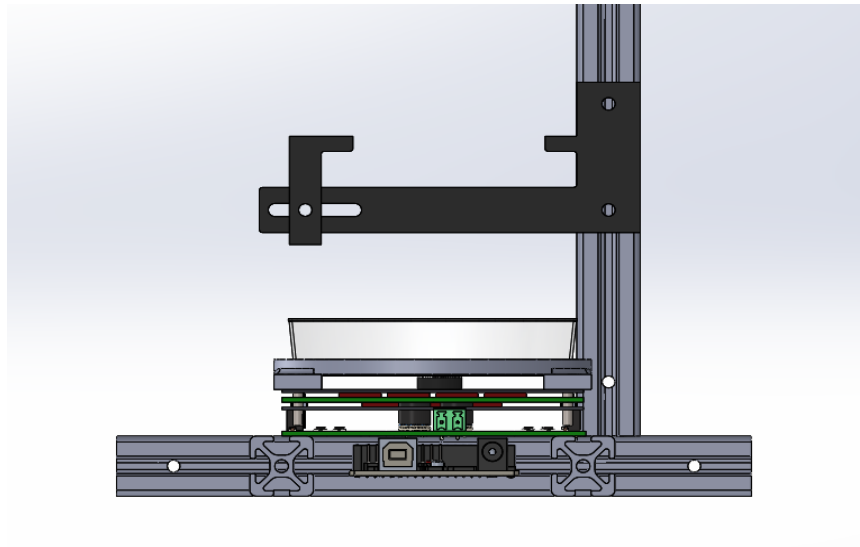
(a)
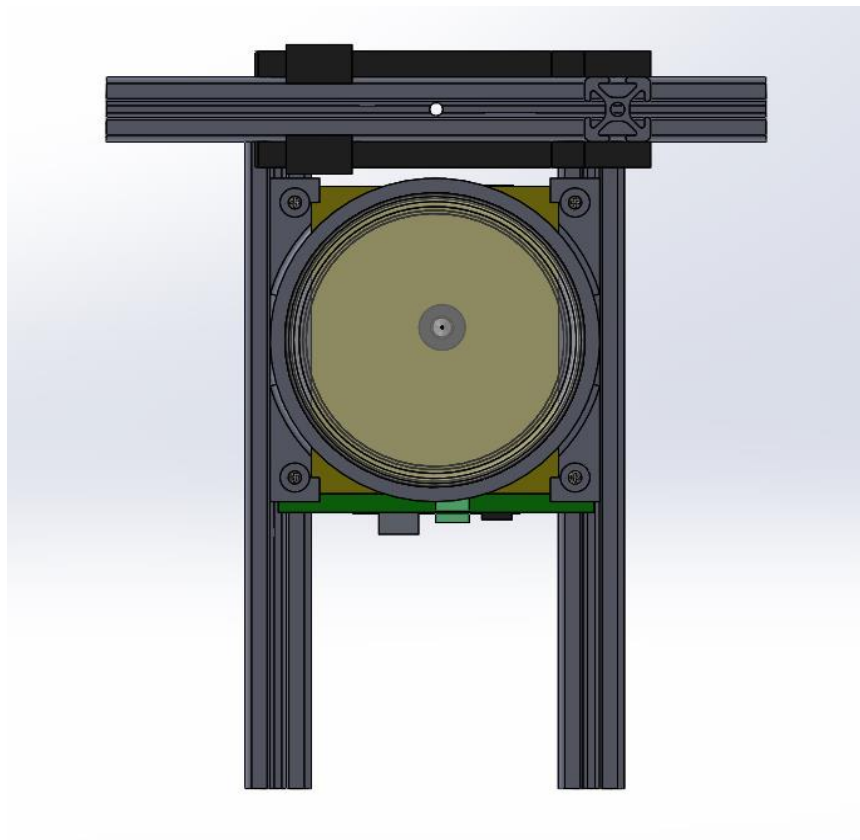
(b)

Figure 4.12: System assembly, side view (a), top view (b)

Petri dishes with a diameter of 100 mm were used as the working area. The reason for using a Petri dish is that the dish is transparent and a structure is needed to hold the lubricant oil. The petri dish is fixed with the petri dish holder attached to the PCB assembly.

Chapter 5

5. Software

To fulfil the scenarios, a software was developed in C++ language using the "Arduino 1.5.2" program on the "Atmega 2560" microcontrollers. Three different algorithms work in the microcontrollers. These are power control, macro position and micro position control algorithms. The power control algorithm was designed to bring the magnetic fields produced by the coils in the upper and lower layers to equal sizes. Macro and micro position algorithms were designed to drive the microrobot to the desired positions. The microcontrollers receives the commands via USB connected to the computer and works. The software is explained in the following subsections.

5.1 Coil Power Control Using PWM

It was validated with the measurements that the coils they have a series resistance of about 1 Ω. Coil connection paths on the PCB and serial equivalent resistances of the connectors are also included in this series resistor. Also, when the designed driver circuit is examined, a low-side mosfet transistor is used to drive each coil, the transistor acts as a switch at this point, completing the circuit and allowing current to flow through the coil. However, this coil driving method makes it difficult to control the current flowing directly over the coil and indirectly the magnetic field produced by the coil. In order to overcome this situation, the coils are driven by pulse width modulation technique.
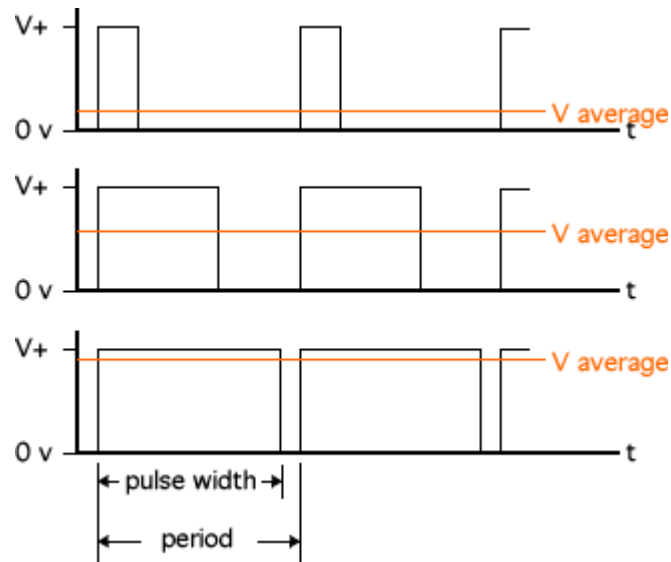
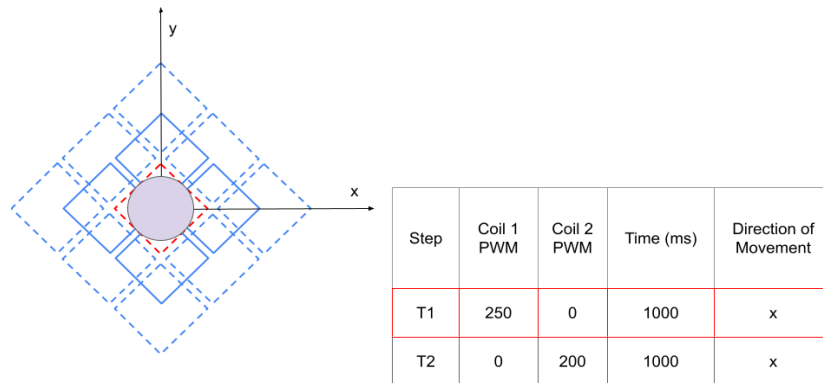Figure 5.1: PWM representation and average voltage [23]

Pulse width modulation (PWM,) is a method of controlling the average power transmitted by an electrical signal. As shown in Figure. 5.1, the average value of the voltage supplied to the load is controlled by changing the source from 0% to 100% at a rate faster than necessary for the load to change significantly, in other words, when the PWM frequency is kept higher than the maximum frequency that the system can reach, the system response operates according to the average of the input. The longer the switch stays open, the higher the total power supplied to the load.

In addition to the PWM drive method for coil power control, the input voltage must be actively controlled. The reason is that the average voltage sent to the coils after PWM changes with the change of the input voltage and is due to the open loop operation of the control algorithm. To avoid this problem, the input voltage supplied to the system should be kept as constant as possible and the output impedance of the power supply should be kept as low as possible.

5.2 Macro Positioning

Two different position control algorithms were developed for the position control of the car circulating on the coil matrix. The first one is the control algorithm, which

can be call rough position control. It is used in situations that do not need precise positioning but require rapid repositioning of the car and the upper load.

Step	Coil 1 PWM	Coil 2 PWM	Time (ms)	Direction of Movement
T1	250	0	1000	x
T2	0	200	1000	x

(a)

Step	Coil 1 PWM	Coil 2 PWM	Time (ms)	Direction of Movement
T1	250	0	1000	x
T2	0	200	1000	x

(b)

Step	Coil 1 PWM	Coil 2 PWM	Time (ms)	Direction of Movement
T1	250	0	1000	x
T2	0	200	1000	x
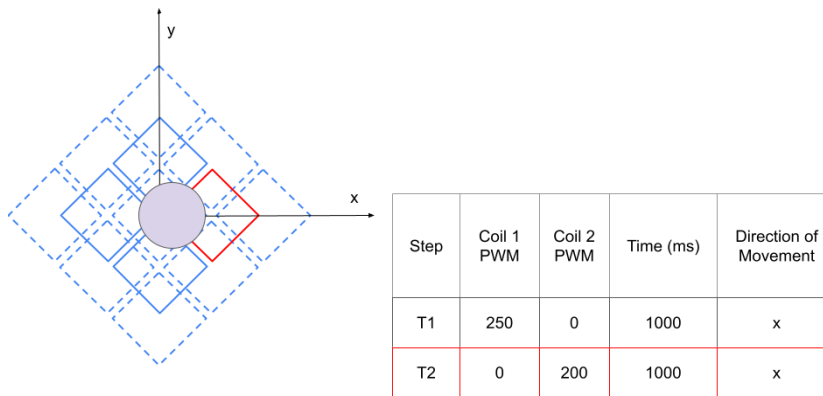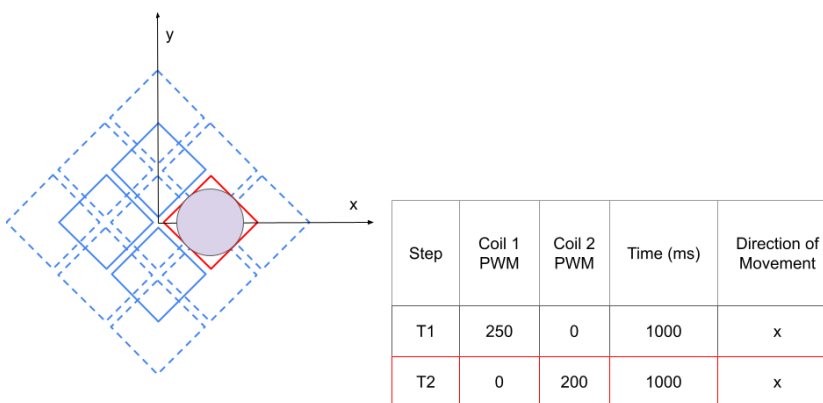
(c)

Figure 5.2: (a, b, c) Macro position control visualization diagrams.

The operating logic of this control method is shown in Figure. 5.2. As seen, the coils are energized in sequence and the car is expected to move from one coil center to the other coil center. The distance between the steps is 10 mm and, in this mode, the PCB actuator works like a stepper motor.

5.2 Micro Positioning

Micro position control algorithms were developed for precise positioning. With this control method, intermediate movement distances can be achieved instead of the 10 mm step distance in the coarse movement function. In this algorithm, the coil in the goal position direction is energized with a very short-term electrical pulse, then this energy is cut off immediately. The width of this pulse must be small enough to overcome the friction between the magnet and the surface and give a very small speed. When the energy is cut off, the magnetic force applied to the magnet is interrupted, and its speed drops to zero due to the friction force.
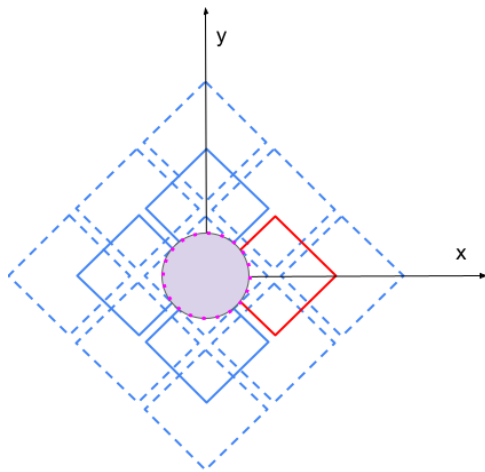
Step	Coil 1 PWM	Coil 2 PWM	Time (ms)	Direction of Movement
T1	0	200	1	x
T2	0	0	10	x
T3	0	200	1	x
T4	0	0	10	x

(a)
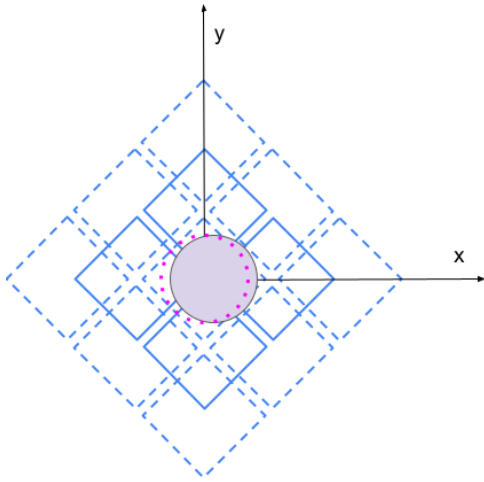
Step	Coil 1 PWM	Coil 2 PWM	Time (ms)	Direction of Movement
T1	0	200	1	x
T2	0	0	10	x
T3	0	200	1	x
T4	0	0	10	x

(b)

Step	Coil 1 PWM	Coil 2 PWM	Time (ms)	Direction of Movement
T1	0	200	1	x
T2	0	0	10	x
T3	0	200	1	x
T4	0	0	10	x

(c)

53
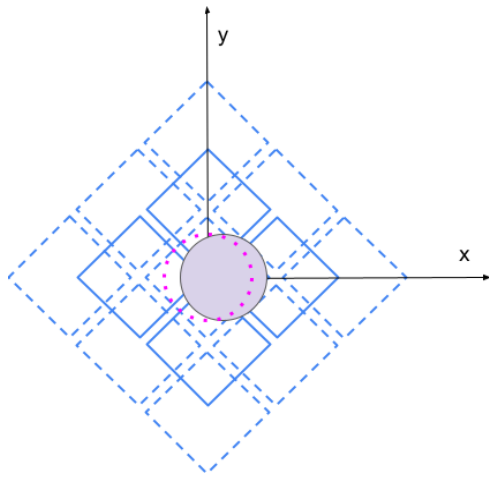
Step	Coil 1 PWM	Coil 2 PWM	Time (ms)	Direction of Movement
T1	0	200	1	x
T2	0	0	10	x
T3	0	200	1	x
T4	0	0	10	x

(d)

Figure 5.3: (a, b, c, d) Micro position control visualization diagrams.

In Figure 5.3, goal position is in the x-axis, the coil indicated in red is the coil closest to the magnet in the direction of movement. This coil is energized for 1 ms at the T1 step. Just after the magnet starts to move, the coil energy is cut off for 10 ms at the T2 step. After the magnet movement energy is damped due to friction, it is energized again for 1 ms at the T3 step, and the steps continue one after another until they reach the target position. Energizing and de-energizing time intervals were found experimentally. In addition, since the force acting on the magnet depends on the distance between the coil and the magnet, the blow given in every position and the movement distance are not equal. In order to overcome this problem, closed-loop control with the help of a camera is required.

Chapter 6

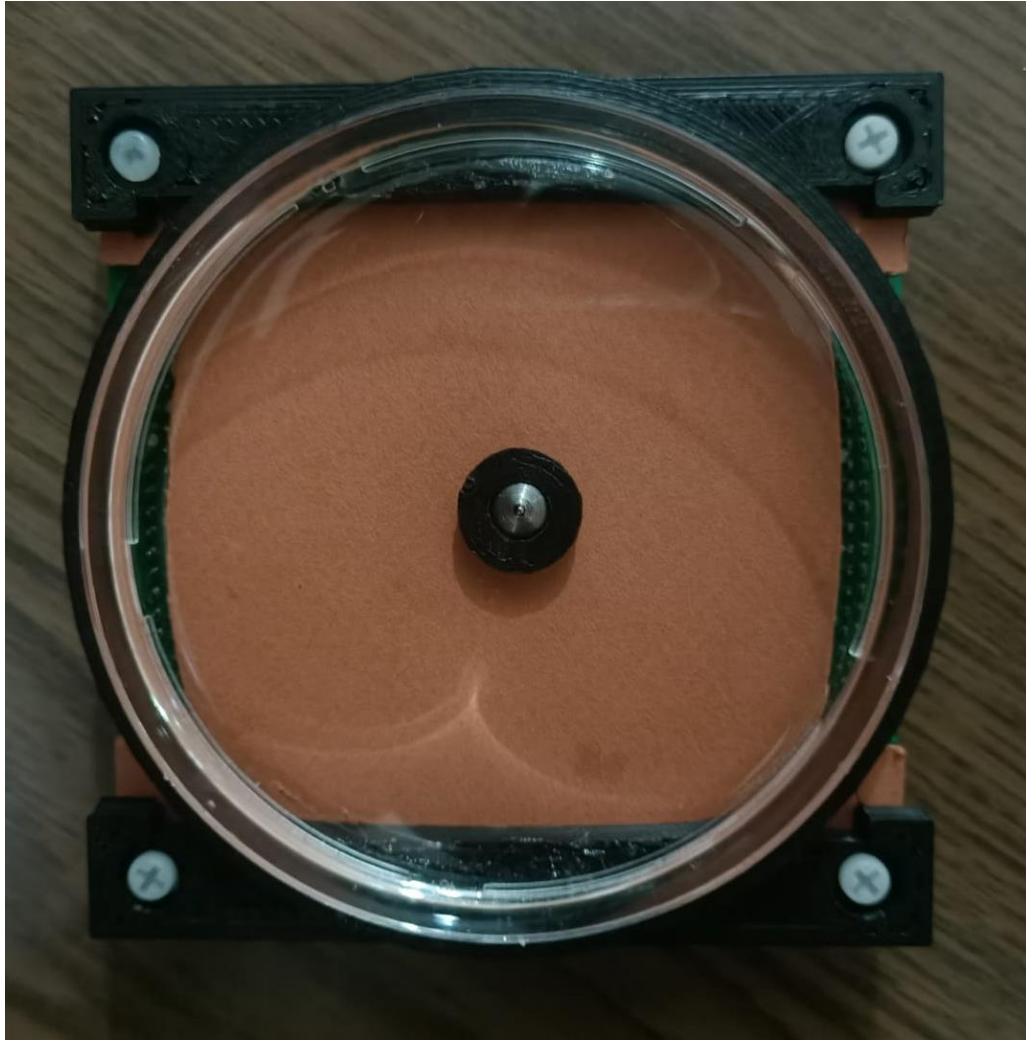# 6. Experimental Results

6.1 PCB-Based Electromagnetic Actuator System Installation

To tests of the designed electromagnetic actuator system and to analysis motion of the microrobot, a test system was produced. The main parts that make up the test system are shown in Figure 6.1. All the parameters that make up the electromechanical structure are included in the system design, as stated.
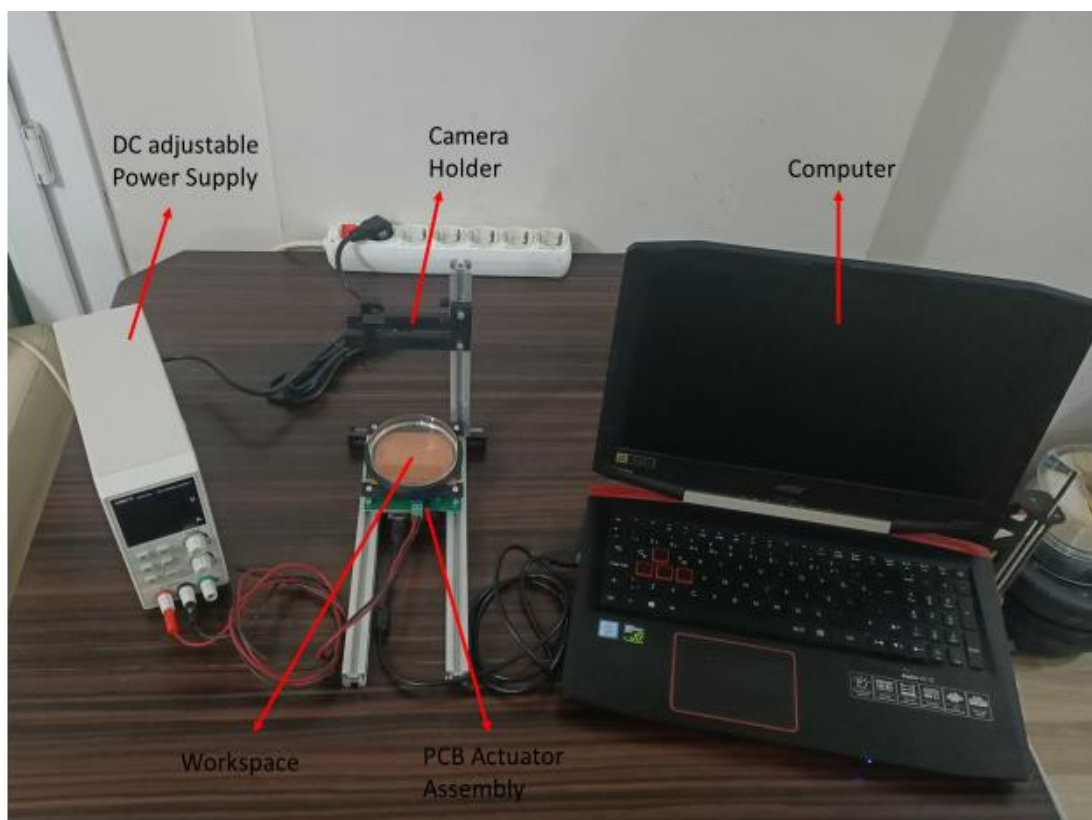
(a)

(b)

Figure 6.1: PCB-based electromagnetic actuator system installation(a,b).

Figure 6.2 shows the working princible of the experimental system. The control methodolgy of the system is open-loop control. The operator constantly monitors the position of the microrobot via the camera. The operator enters control commands to the computer according to the movement function according to the position information of the microbot. The computer sends the given commands to the microcontroller with the help of USB. The commands are evaluated in the control loop and transferred to the driver cards with the motion functions previously defined and loaded into the microcontroller. The position and current control of the electromagnetic poles are realized by shaping the electric current sent to the actuators by the driver cards.
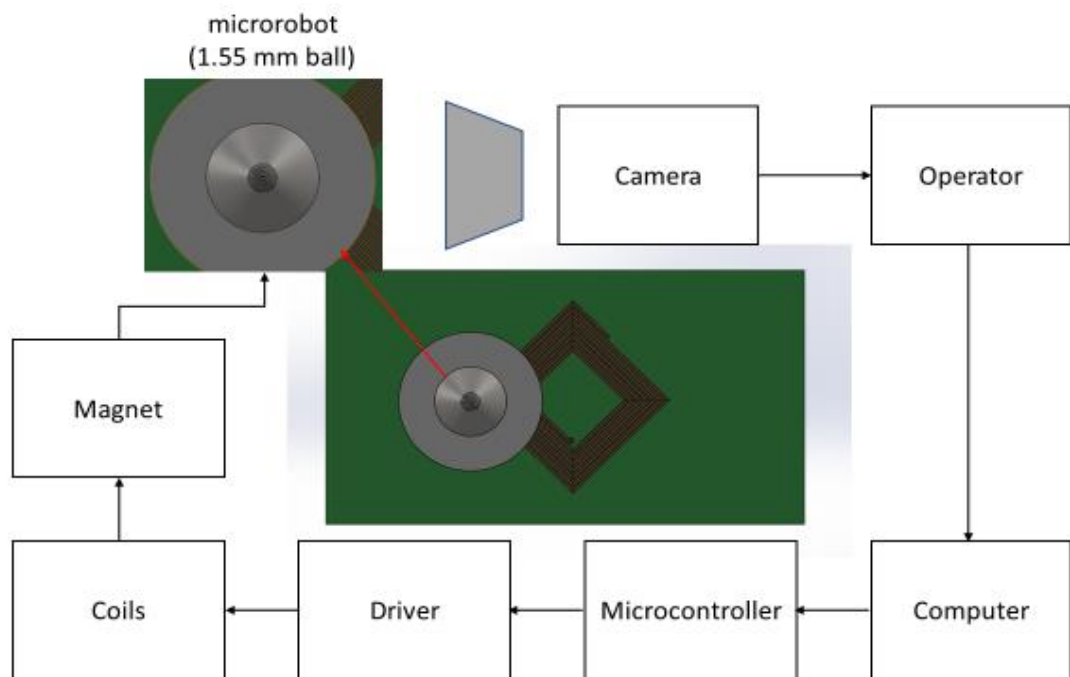
Figure 6.2: Working principle of PCB electromagnetic actuator system.

6.2 Investigation of Planar Motion of Microrobot

As mentioned in the control algorithms in chapter five, the microrobot has two types of motion features. i.e., macro and micro precision. In macro movement, speed and relatively high mobility are aimed, while in micro movement, sensitivity at low speed is aimed. These two types of motion functions are examined in the following headings.

6.2 Investigation of Planar Macro Motion of Microrobot

The initial position of the microrobot in the horizontal xy plane within the determined working limits (75x75 mm) is shown in Figure 6.3. The size of the squares on the checkered paper affixed to the bottom of the work area is 4x4 mm.

Figure 6.3: The initial position of the microrobot in the xy horizontal plane.
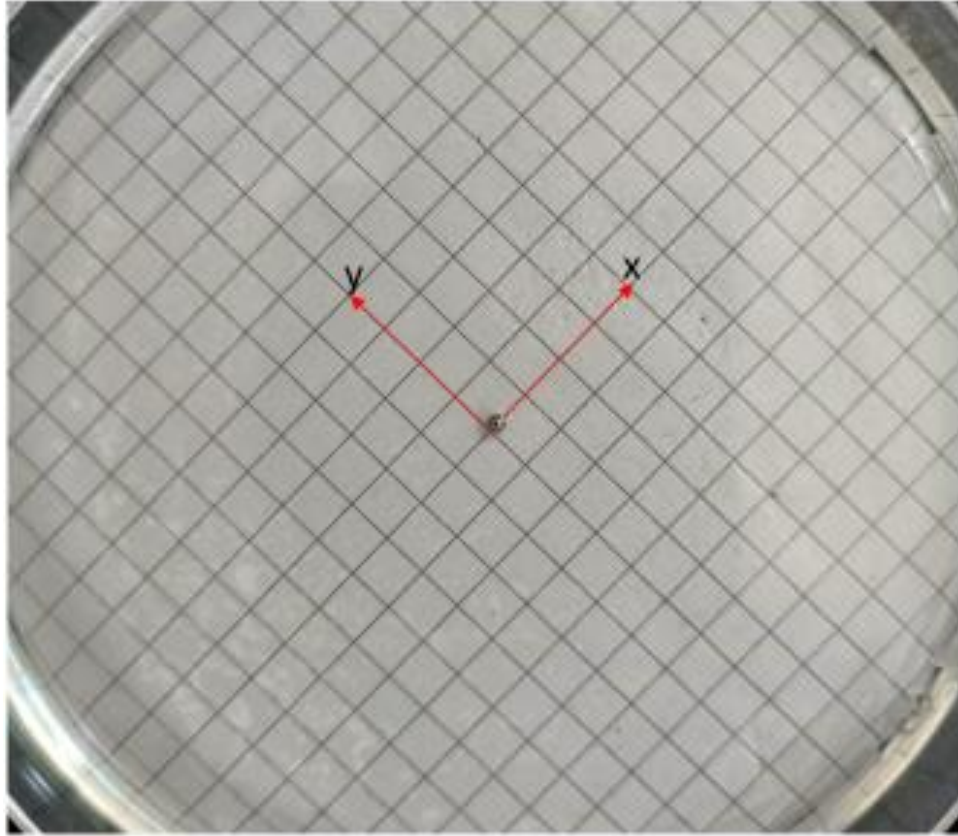
The study aims to test the macro mobility of the microrobot within the working limits. For this purpose, movements were made by using the motion setup determined by the microrobot.

The microrobot was first brought to the 0 position by energizing the coil in the origin. The targeted direction is +x direction and the microrobot is aimed to advance 10 mm. In order to provide this movement, the neighbouring coil of the center coil in the +x direction is energized, while all other coils are closed. The magnetic field produced by the coil in the +x direction interacts with the magnet in the car under the working area and attracts the magnet to the coil. The car interacts with the microrobot and pulls the microrobot to the target location. 10mm orientation of the microrobot in the +x direction and Macro movement Figure 6.4 is also shown.

(a)   (b)

Figure 6.4: (a, b) 10mm orientation and linear movement of the microrobot in the +x direction.

6.2 Investigation of Planar Macro Motion of Microrobot

The initial position of the microrobot in the horizontal xy plane within the determined working limits (75x75 mm) is shown in Figure 6.5. The size of the squares on the checkered paper affixed to the bottom of the work area is 4x4 mm.
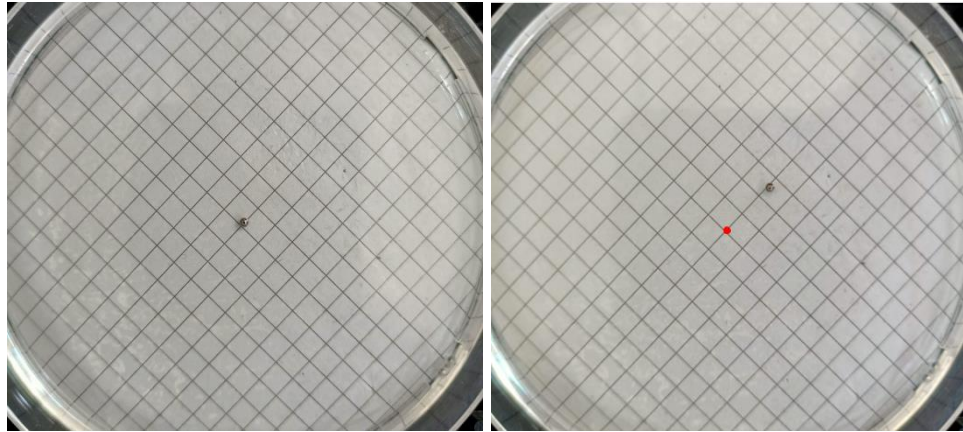
Figure 6.5: The starting position for micromovement of the microrobot in the xy horizontal plane(x and y axis as in Figure 6.3).

The study aims to test the microrobot's ability to move within a 10x10 mm area around the origin. For this purpose, movements were made by using the motion setup determined by the microrobot. An important point to be noted is that the actuator microrobot can be moved at a micro level throughout the working volume, and the images have been reduced to show the operation of the system.

The microrobot was first brought to the O position by energizing the coil in the origin. The targeted direction is +X direction, and it is aimed to progress by making small steps of the microrobot 8 mm movement. In order to ensure this movement, the neighbouring coil of the center coil in the +X direction is energized with the micro position control function, while all other coils are in the closed state. The magnetic field produced by the coil in the +X direction interacts with the magnet in the car under the working area and attracts the magnet to the coil. The car interacts with the microrobot and pulls the microrobot to the target location. Orientation of the microrobot in the +X direction a few mm and Micro movement Figure 6.6 is also shown.

(a)

(b)

(c)

(d)

(e)

Figure 6.6: Orientation and linear movement of the microrobot in the +X direction with 8mm micro steps (a, b, c, d, e).

As seen in Figure 6.6, the microrobot can be taken to any desired point between two coils (10mm) with the micro position control technique.

6.3 Investigation of Step Response of Actuator with 1.55 mm Microrobot

The step response of a 2D actuator refers to its behaviour when subjected to a sudden change or step input in the desired position. When a step input is applied, the actuator rapidly adjusts its position in both the x and y axes to reach the new setpoint. The response time of the actuator, known as the settling time, is a measure of how quickly it achieves stability after the step input. A fast-settling time indicates a highly responsive actuator, capable of swiftly adapting to new position commands.

1.55 mm actuator is set to follow a trajectory in the test setup as given in Figure 6.7. The desired trajectory is 10 mm straight line. Movement of the microrobot was observed using a camera and displacement was obtained using image processing. Video captured in a format that; 1080p and 120Hz.
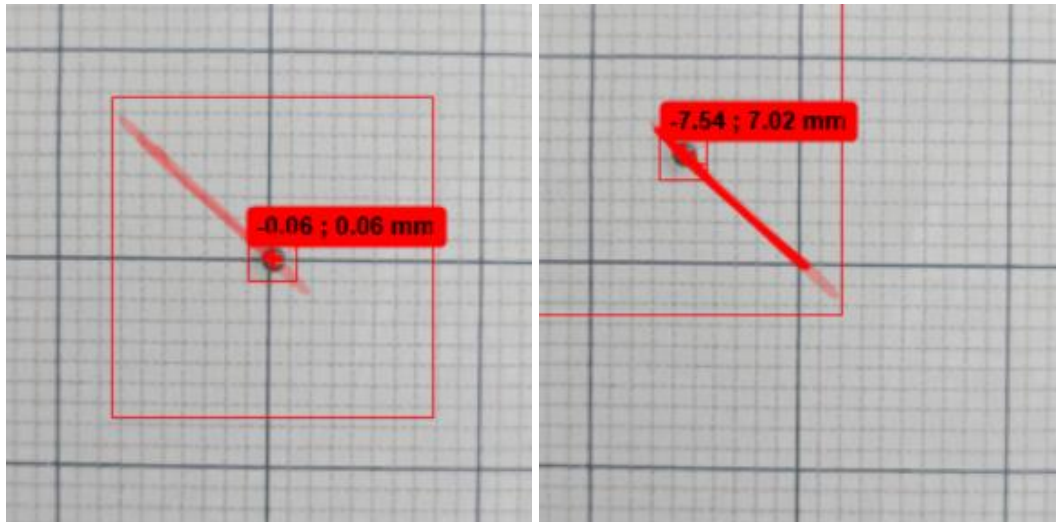
(a)   (b)

Figure 6.7: Test stup for video prossesing, (a) beginning and (b) final position.
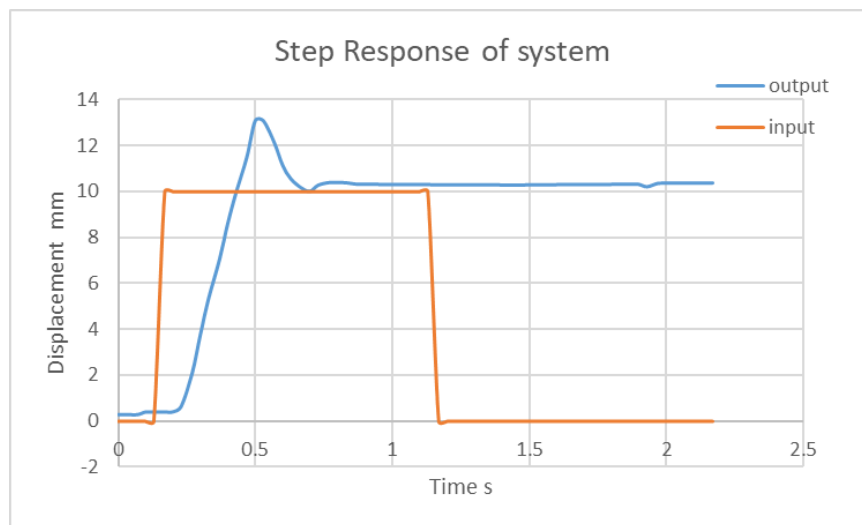

Figure 6.8: Step response of the 1.55mm microrobot.

Figure 6.8 shows the response of the 1.55mm   10 mm step input with 1000 ms
duration. Since the system works like a 2D stepper motor in macro motion function,

there is no need for a closed-loop control algorithm. In the test model, the coil, which is 10 mm away from the microbot at the origin (ie on the central coil), is energized for 1000 ms and the movement of the microrobot is examined with the help of a camera. The microrobot responds approximately 100 ms after input and its rise time is 200 ms. The microrobot shows the underdamped system characteristic and oscillates until it reaches the steady state. When the graph is examined, it makes approximately 30% overshoot.

6.4 Investigation of Step Response of Actuator with 0.79 mm Microrobot

0.79 mm actuator is set to follow a trajectory in the test setup as given in Figure 6.9. The desired trajectory is 10 mm straight line. Movement of the microrobot was observed using a camera and displacement was obtained using image processing. Video captured in a format that; 1080p and 120Hz.
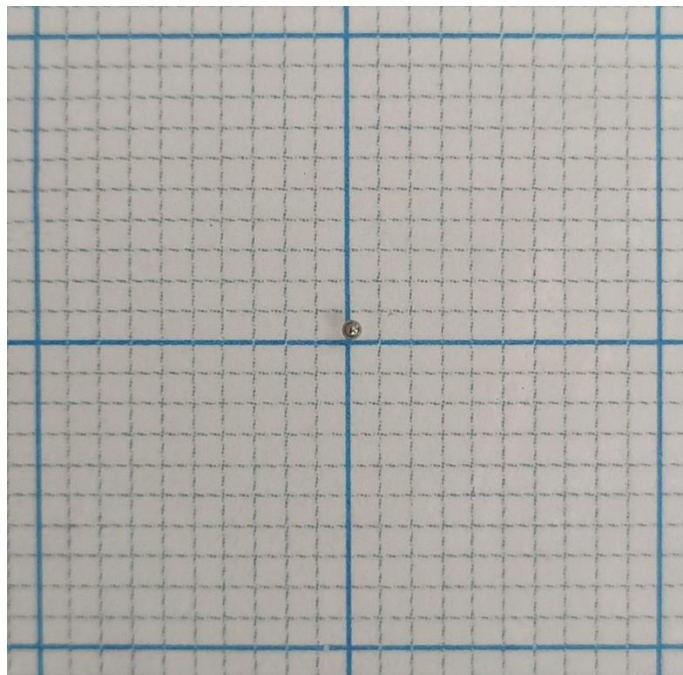

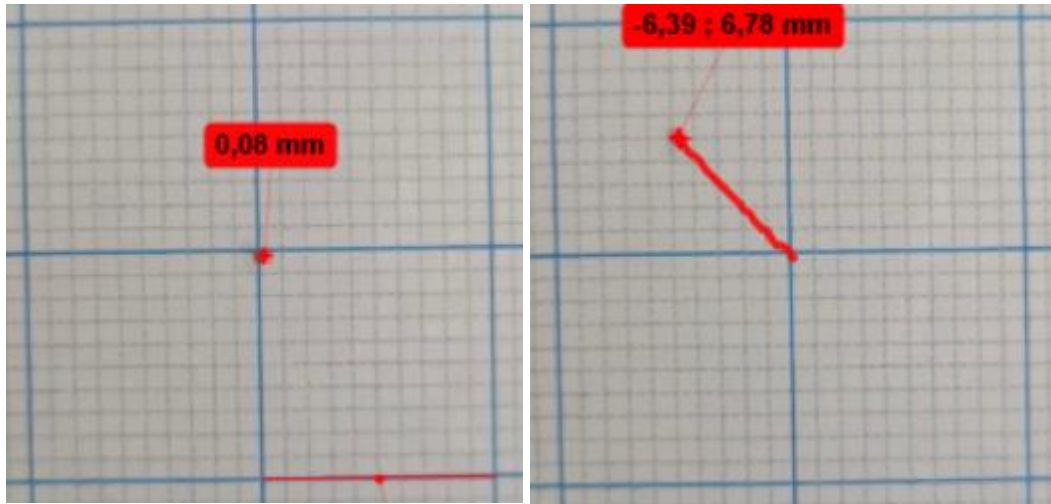Figure 6.9: 0.9 mm microrobot at the origin.

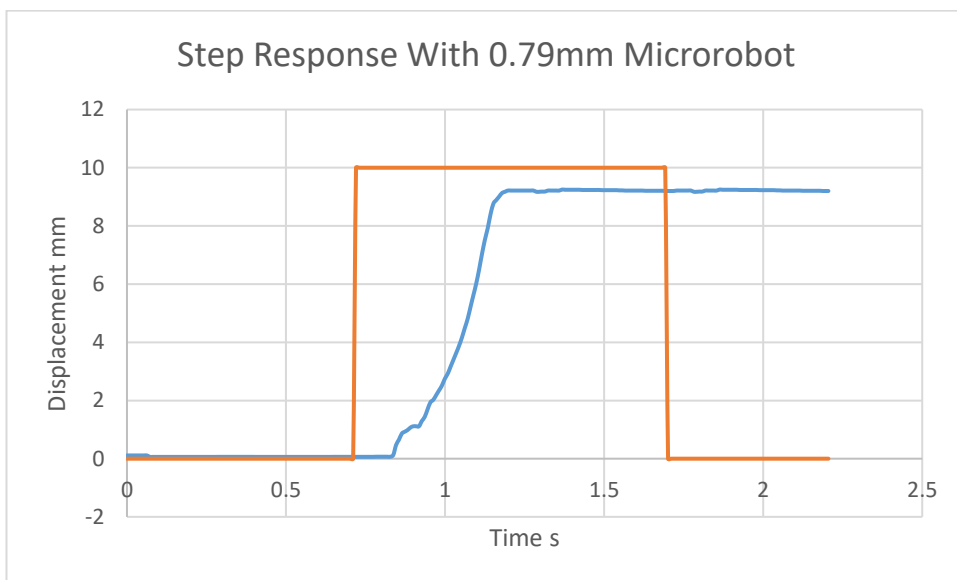Figure 6.10: Test setup for video processing, beginning(a) and final(b) position.

Figure 6.11: Step response of the 0.79 mm microrobot.

Figure 6.9 shows the 0.79 mm microrobot to 10 mm step input with 1000 ms duration. Results show that this size not enough to actuator locote the micro robot pricesly.

6.5 Investigation of Repeatability of Actuator with 1.55 mm Microrobot

The repeatability of an actuator is a critical characteristic that determines its ability to reproduce a desired motion or position consistently and accurately. Repeatability refers to the actuator's ability to return to the same position or follow the same trajectory repeatedly under similar operating conditions. It is influenced by various factors, including mechanical precision, control algorithms, sensor accuracy, and environmental conditions. Actuators with high repeatability are essential in applications that require precise and reliable positioning, such as robotics, manufacturing automation, and precision instrumentation. Manufacturers often specify the repeatability of an actuator as a percentage or an absolute value, indicating the maximum allowable deviation from the desired position. Achieving high repeatability typically involves careful design, tight manufacturing tolerances, accurate sensing, and robust control strategies.

1.55 mm actuator is set to follow the same trajectory repeatedly. The desired trajectory is 10 mm straight line, the microrobot follows same trajectory and comes back to its origin. Movement of the microrobot was observed using a camera and displacement was obtained using image processing. Video captured in a format that; 1080p and 120Hz.
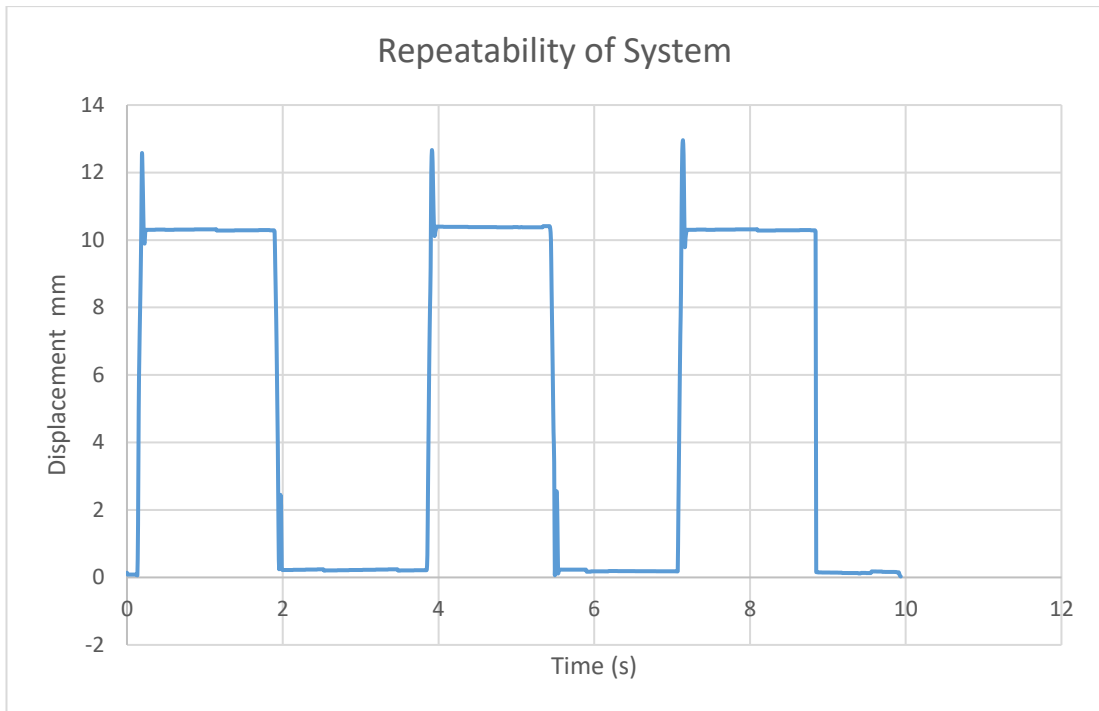
Figure 6.12: Repeatability of the system.

Figure 6.9 shows the displacement of the microrobot in this test. After gathering the data from the actuator output and calculation, results show that the actuator has 0.12 mm uncertainty in its motion. And experiments show that uncertainty highly depends on direction of motion.

Chapter 7

7. Conclusion and Recommendations

As expected, PCB coils create a magnetic field like small electromagnets, and with the magnetic field they produce, they can create a pulling force of 300~350 mN on a 12x2 mm Neodymium magnet 1mm above the PCB coil center and attract the magnet 5-6 mm away from the center of PCB coil. The fact that pulling force gradually decreases with distance as the magnet gets away from the PCB coil, at which point the coil is no longer able to attract the magnet due to friction force. That means to enlarge a suitable working area, the friction force between that one face of the magnet and the surface of the bed needs to be precisely controlled. And fraction force can be compensated by increasing the pulling force created by the PCB coil with the increasing operating current.

As in the PCB actuator calculations presented in this study, the microrobot can be moved at macro and micro levels in the directions where the coils overlap. The macro movement is in the x or y axis and the distance between the coils is about 10 mm. Micro motion can be provided in any desired resolution between the coils. However, since PCB coils produce weak magnetic fields, they cannot attract the magnet to themselves without surface overlap. For this reason, the magnet can only move in the directions that overlap with the coil. When the diameter of the magnet is increased to increase the overlap, the net force on the magnet decreases and limits the mobility of the actuator. To overcome this problem, coils designed to produce stronger magnetic fields can be designed or the mobility can be increased by changing the coil types.

The 1.55 mm diameter bearing ball, which is selected as a microrobot, is a little too big for this task. Other smaller bearing balls on the market are 0.79 mm. In the experiments, it was determined that the magnet and magnetic core structure could not

confine the small ball to the magnetic field like the other large ball, and there was an uncertainty in the microrobot movement. To overcome this problem, it is necessary to find more magnetic particles or to assemble a car with a stronger magnetic field.

References

[1] Wang, W., Zhou, C., "A Journey of Nanomotors for Targeted Cancer Therapy: Principles, Challenges, and a Critical Review of the State-of-the-Art," Adv. Healthcare Mater., vol. 10, no. 2, 2001236, 2021. https://doi.org/10.1002/adhm.202001236

[2] M. Zhang, L. Yang, C. Zhang, Z. Yang and L. Zhang, "A 5-D Large-Workspace Magnetic Localization and Actuation System Based on an Eye-in-Hand Magnetic Sensor Array and Mobile Coils," in IEEE Transactions on Instrumentation and Measurement, vol. 72, pp. 1-11, 2023, Art no. 7501411, https://doi.org/10.1109/TIM.2023.3238693

[3] B. Ahmad, M. Gauthier, G. J. Laurent and A. Bolopion, "Mobile Microrobots for In Vitro Biomedical Applications: A Survey," in IEEE Transactions on Robotics, vol. 38, no. 1, pp. 646-663, Feb. 2022, https://doi.org/10.1109/TRO.2021.3085245

[4] Shi-Chune Yao, Xudong Tang, Cheng-Chieh Hsieh, Yousef Alyousef, Michael Vladimer, Gary K. Fedder, Cristina H. Amon, "Micro-electro-mechanical systems (MEMS)-based micro-scale direct methanol fuel cell development," vol. 31, no. 5, pp. 636-649, April 2006. https://doi.org/10.1016/j.energy.2005.10.016

[5] B. Ahmad, A. Barbot, G. Ulliac and A. Bolopion, "Hybrid Optothermal-Magnetic Mobile Microgripper for In-Liquid Micromanipulation," in IEEE Robotics and Automation Letters, vol. 8, no. 3, pp. 1675-1682, March 2023. https://doi.org/10.1109/LRA.2023.3242168

[6] D. Rivas, S. Mallick, M. Sokolich and S. Das, "Cellular Manipulation Using Rolling Microrobots," 2022 International Conference on Manipulation, Automation and Robotics at Small Scales (MARSS), Toronto, ON, Canada, pp. 1-6, 2022. https://doi.org/10.1109/MARSS55884.2022.9870486

[7] Vincent Vandaele, Pierre Lambert, Alain Delchambre, "Non-contact handling in microassembly: Acoustical levitation", Precision Engineering, Volume 29, Issue 4, Pages 491-505,2005, ISSN 0141-6359, https://doi.org/10.1016/j.precisioneng.2005.03.003.

[8] W. Jung, S. Lee, J. Lee and Y. Hwang, "Wirelessly Powered Micro Soft Bellows Actuator with 3D Helix Coils," 2022 IEEE 35th International Conference on Micro Electro Mechanical Systems Conference (MEMS), Tokyo, Japan, pp. 361-364, 2022. https://doi.org/10.1109/MEMS51670.2022.9699778

[9] M. Meng, A. Ibrahim and M. Kiani, "Design considerations for ultrasonic power transmission to millimeter-sized implantable microelectronics devices," 2015 IEEE Biomedical Circuits and Systems Conference (BioCAS), Atlanta, GA, USA, pp. 1-4, 2015. https://doi.org/10.1109/BioCAS.2015.7348295

[10] Chungseon Yu, Juhyun Kim, Hyunchul Choi, Jongho Choi, Semi Jeong, Kyoungrae Cha, Jong-oh Park, Sukho Park, "Novel electromagnetic actuation

system for three-dimensional locomotion and drilling of intravascular microrobot," Sensors and Actuators A: Physical, vol. 161 issues 1–2, pp. 297-304, 2010. https://doi.org/10.1016/j.sna.2010.04.037

[11] Fan, Xinjian et al. "Reconfigurable multifunctional ferrofluid droplet robots." Proceedings of the National Academy of Sciences of the United States of America vol. 117,45 pp. 27916-27926, (2020). https://doi.org/10.1073/pnas.2016388117

[12] G. A. Türkmen, S. Doğanay, L. Çetin and A. Turgut, "Ferrofluid Droplet Robot Manipulation Using Rule-Based Control Strategy," 2022 IEEE XVIII International Conference on the Perspective Technologies and Methods in MEMS Design (MEMSTECH), Polyana (Zakarpattya), Ukraine, pp. 16-19, 2022. https://doi.org/10.1109/MEMSTECH55132.2022.10002916

[13] P. Punyabrahma, G. R. Jayanth and A. K. Mohanty, "Trapping and 3-D Manipulation of Magnetic Microparticles Using Parametric Excitation," in IEEE Robotics and Automation Letters, vol. 7, no. 2, pp. 1403-1407, April 2022, https://doi.org/10.1109/LRA.2021.3138164

[14] Nam-Trung Nguyen, Xiaoyang Huang, "Miniature valveless pumps based on printed circuit board technique",Sensors and Actuators A: Physical, Volume 88, Issue 2, Pages 104-111, ISSN 0924-4247, 2001. https://doi.org/10.1016/S0924-4247(00)00500-8.

[15] Aldoumani, Maha, Baris Yuce, and Dibin Zhu, "Using the Variable Geometry in a Planar Inductor for an Optimised Performance" Electronics vol. 10, no. 6, 2021. https://doi.org/10.3390/electronics10060721

[16] Y. Shi, Z. Xin, P. C. Loh and F. Blaabjerg, "A Review of Traditional Helical to Recent Miniaturized Printed Circuit Board Rogowski Coils for Power-Electronic Applications," in IEEE Transactions on Power Electronics, vol. 35, no. 11, pp. 12207-12222, Nov. 2020. https://doi.org/10.1109/TPEL.2020.2984055

[17] Chowdhury, Sagar & Jing, Wuming & Cappelleri, David. "Towards Independent Control of Multiple Magnetic Mobile Microrobots". Micromachines. 7. 3. 10.3390/mi7010003, 2015. https://doi.org/10.3390/mi7010003

[18] R. Zhang, D. Zhang and R. Dutta, "Study on PCB Based Litz Wire Applications for Air-Core Inductor and Planar Transformer," 2019 9th International Conference on Power and Energy Systems (ICPES), Perth, WA, Australia, pp. 1-6, 2019. https://doi.org/10.1109/ICPES47639.2019.9105549

[19] Faria, Andreia, Luís Marques, Carlos Ferreira, Filipe Alves, and Jorge Cabral. 2021. "A Fast and Precise Tool for Multi-Layer Planar Coil Self-Inductance Calculation" Sensors 21, no. 14: 4864. https://doi.org/10.3390/s21144864

[20] Bhattacharjee, A., Rogowski, L. W., Zhang, X., & Kim, M. J. "Untethered soft millirobot with magnetic actuation". In 2020 IEEE International Conference on Robotics and Automation (ICRA) pp. 3792-3798, 2020, May. https://doi.org/10.1109/ICRA40945.2020.9197202

[21] IPC ASSOCIATION CONNECTING ELECTRONICS INDUSTRIES, "IPC-2221A Generic Standard on Printed Board Design," February 1998. http://www-eng.lbl.gov/~shuman/NEXT/CURRENT_DESIGN/TP/MATERIALS/IPC-2221A(L).pdf

[22] Serkan Doganay, Alpaslan Turgut, Levent Cetin, "Magnetic field dependent thermal conductivity measurements of magnetic nanofluids by 3ω method". Journal of Magnetism and Magnetic Materials, Volume 474, Pages 199-206, ISSN 0304-8853, 2019. https://doi.org/10.1016/j.jmmm.2018.10.142.

[23] https://electronics.stackexchange.com/questions/128804/generating-a-variable-dc-signal-with-pwm

Appendices

Appendix A

Publications from the Thesis

Journal Articles

1. Comparison of PCB Based Actuator Coils for Untethered Actuation

Republic of Turkey

İzmir Kâtip Çelebi University

Graduate School of Natural and Applied Sciences

Printed Circuit Board Coil Based Electromagnetic Actuator Design For Micro/Miliscale Manipulation

Department of Robotics Engineering

Master's Thesis

Erdem Doguş AKKUŞ

ORCID 0009-0001-6783-3125

Thesis Advisor: Prof. Dr. Levent ÇETİN

July 2023

74

Curriculum Vitae

Name Surname   : Erdem Doğuş AKKUŞ

E-mail (1)   : 150412012@ikcu.ogr.edu.tr

E-mail (2)   : e.dogus.akkus@gmail.com

Education:

2015–2020	İzmir Kâtip Çelebi University, Dept. of Mechatronics Eng.
2020–2023	İzmir Kâtip Çelebi University, Dept. of Robotics Eng.

Work Experience:

2020 – 2022	MND İzolasyon LTD. STİ.
2022 – 2023	GTM Europe LTD. STİ.
2023 –	Vestel AŞ.

Publications (if any):

1. Comparison of PCB Based Actuator Coils for Untethered Actuation